Epigenomic landscape of the human dorsal root ganglion: sex differences and transcriptional regulation of nociceptive genes

Running title: epigenome of the human DRG

Úrzula Franco-Enzástiga[1], Nikhil N. Inturi[1], Keerthana Natarajan[1], Juliet M. Mwirigi[1], Khadija Mazhar[1], Johannes C.M. Schlachetzki[2], Mark Schumacher[3], Theodore J. Price[1,*]

[1] Center for Advanced Pain Studies, School of Behavioral and Brain Sciences, University of Texas at Dallas, Richardson, Texas 75080.

[2] Department of Cellular and Molecular Medicine, University of California, San Diego, 9500 Gilman Drive, La Jolla, CA 92093-0651, USA.

[3] Department of Anesthesia and Perioperative Care and the UCSF Pain and Addiction Research Center, University of California, San Francisco, California, 94143 USA.

[*]Correspondence to:

Theodore J Price PhD
800 W Campbell Rd
BSB14.102
Richardson TX 75080
USA
theodore.price@utdallas.edu
+1 972-883-4311

Word count: 11,345
Abstract: 227
Significance Statement: 114
Document: 1
Number of Text Pages: 38
Number of Figures: 7 (Supplementary figures: 5)
Number of Tables: 0 (Supplementary tables: 9)

Classification - Neuroscience, Genetics

Key words - epigenetics, chromatin, dorsal root ganglion, ATAC-seq, sex differences, EGR transcription factor, SP transcription factor, AP-1 transcription factor

Author Contributions – UFE and TJP designed research project; UFE conducted ATAC-seq and RNA-seq experiments; UFE, NNI, and JCMS performed computational analysis; UFE designed and KN performed *in situ* hybridization experiments; JM and KM supplied computational feedback; JCMS and MS provided insight to the paper; UFE and TJP wrote the paper.

Competing Interest Statement - The authors declare no financial conflicts of interest related to this work.

Abstract:

Gene expression is influenced by chromatin architecture via controlled access of regulatory factors to DNA. To better understand regulation of gene expression in the human dorsal root ganglion (hDRG) we used bulk and spatial transposase-accessible chromatin technology followed by sequencing (ATAC-seq). We detected a total of 3005 differentially accessible chromatin regions (DARs) between sexes using bulk ATAC-seq. DARs in female hDRG mapped mainly to the X chromosome. In males, DARs were found in autosomal genes. We also found differential transcription factor binding motifs within DARs. EGR1/3 and SP1/4 were abundant in females, and JUN, FOS and other AP-1 family members in males. With the aim of dissecting the open chromatin profile in hDRG neurons, we used spatial ATAC-seq. Consistent with our bulk ATAC-seq data, most of the DARs in female hDRG were located in X chromosome genes. Neuron cluster showed higher chromatin accessibility in GABAergic, glutamatergic, and interferon-related genes in females, and in Ca^{2+}-signaling-related genes in males. Sex differences in open chromatin transcription factor binding sites in neuron-proximal barcodes were consistent with the bulk data, having EGR1 transcription factor activity in females and AP-1 family members in males. Accordingly, we showed higher expression of *EGR1* in female hDRG compared to male with in-situ hybridization. Our findings point to epigenomic sex differences in the hDRG that likely underlie divergent transcriptional responses that determine mechanistic sex differences in pain.

Significance Statement:

Women more frequently suffer from chronic pain than men. Animal and human studies demonstrate that underlying molecular mechanisms causing chronic pain differ by sex. We hypothesized that epigenomic differences in the hDRG may underlie both the higher propensity for women to develop chronic pain disorders and mechanistic sex differences in chronic pain. As a first test of this idea, we mapped the open chromatin accessibility landscape of the hDRG in female and male organ donor-recovered tissues. Our findings highlight clear baseline sex differences in the hDRG that provide a mechanistic explanation for how injury and/or inflammation can drive different transcriptional programs that ultimately change the excitability of DRG neurons, creating signals that cause pain.

Introduction

Women exhibit a higher prevalence of chronic pain (1), a greater number of clinical pain conditions (2), and a heightened sensitivity to experimental pain compared to men (3). The strongest evidence is epidemiological and mechanistic sex differences in chronic pain conditions (4-7). Neuropathic, inflammatory and idiopathic chronic pain have higher prevalence rates, symptom severity and duration in women compared to men (6, 8, 9). Although, hormonal, immunological, anatomical and psychosocial factors contribute to sex differences in pain (10), at least some of these differences are likely driven by sex-specific gene expression in sensory neurons, glia or immune cells of the human dorsal root ganglion (hDRG). Support for this idea comes from animal model work demonstrating distinct mechanisms that promote and resolve chronic pain in rodents (11, 12). Mechanistic studies in humans demonstrate sex differences in gene expression for transcription factors and epigenetic remodelers in hDRG from thoracic vertebrectomy patients suffering from chronic pain (13, 14). Moreover, in both the human tibial nerve and in the human DRG, as well as in the mouse DRG, there are sex differences in gene expression in individuals without any pain history suggesting underlying epigenetic differences at baseline that cause these divergent patterns of gene expression (13-19).

Chromatin is a macromolecular complex composed of DNA, RNAs, and proteins found within the nuclear space. Epigenetic marks, such as specific histone or DNA modifications, can affect the degree of DNA compaction resulting either in open or accessible regions termed euchromatin or closed compact regions known as heterochromatin (20). Chromatin accessibility is defined as the extent to which nuclear macromolecules can physically interact with chromatinized DNA (21). Although chromatin serves a structural role by compacting DNA, it is also a dynamic entity that responds to cellular needs such as transcription, DNA repair, and differentiation (22, 23). These dynamic changes in chromatin have been shown in the DRG in animal models in response to nerve injury and to inflammation, demonstrating a functional link between epigenomic regulation of gene expression and development and maintenance of chronic pain (24-31). To date very little is known about chromatin accessibility in

hDRG although one previous study using microarray-based genomic and mRNA expression profiling found that expression quantitative trait loci were associated with open chromatin regions based on encyclopedia of DNA elements datasets (32). A study of the human trigeminal ganglion (TG) found association between single nucleus ATAC-seq (snATAC-seq) open chromatin regions and single nucleotide polymorphisms (SNPs) associated with migraine (33). However, the degree to which SNPs linked to migraine could be correlated to open chromatin in human TG cells was limited because snATAC-seq failed to cover all TG cell types detected with snRNA-seq.

We hypothesized that epigenomic differences in the hDRG may underlie mechanistic differences in molecular events that promote pain in females versus males and contribute to the higher propensity for women to develop chronic pain disorders. As a first test of this idea, we used both bulk and spatial ATAC-seq coupled with bulk nuclear RNA-seq to map the open chromatin accessibility landscape of DRG in female and male organ donor-recovered tissues. We found pervasive differences in transcriptional regulatory programs between females and males that likely have important implications for understanding epidemiological and mechanism-based differences in chronic pain in humans.

Results

Global chromatin landscape in female and male hDRG

To characterize the epigenetic landscape of the hDRG we performed ATAC-seq (34), an unbiased approach to assess chromatin accessibility regions within the genome (35) on lumbar hDRG from 9 donors (N=5 females, N=4 males, **Fig. 1A**). Donor information for all the samples that were used for bulk-ATAC in hDRG is shown in **Supp table 1**. After peak calling, we obtained a total of 669,749 peaks in female and 506,435 in male hDRG datasets. At the global level, the distribution of called peaks in both female and male hDRG samples is concentrated in close proximity to the Transcription Start Site (TSS), with a notable accumulation of ATAC-seq signal directly at the TSS rather than in the immediate vicinity (**Fig. 1B**). The ratio between aggregate distribution of reads

centered around the TSS (± 1 kb) and the signal flanking it is referred to as TSS enrichment (TSSe) score. TSSe is an important quality control parameter in ATAC-seq. We obtained a mean TSSe of 3.17 (**Fig. 1C**) similar to other reports using postmortem tissue (36, 37). Fragments of peaks in peaks (FRiP) defined as the measure of how many of the total reads are located within the peaks was greater than 0.13 in average. By mapping ATAC-seq peaks to genomic regions, we found that ~15% of peaks mapped within the putative promoter, ~40% were in distal intergenic regions, and ~35% were found in introns (**Fig. 1D**). The enrichment of accessible chromatin in intergenic regions suggests that distal regulatory sequences, such as enhancers, non-coding regulatory elements in *cis*, can be accessed to regulate gene expression. In many cases, peaks located mainly in promoters (38), but also those harbored in the gene body (introns and exons) have been found to be good predictors of gene expression (39). However, the proof of concept for the functionality of enhancers is tissue specific and requires further experimentation (40). Since our results show that, at the global level, chromatin accessibility in hDRG showed similar annotation to called peaks between sexes, and the proportion was typical to other ATAC-seq reports (41), we aimed to conduct a sex-specific analysis identifying specific genes to investigate whether sex differences in pain could be associated with chromatin structure.

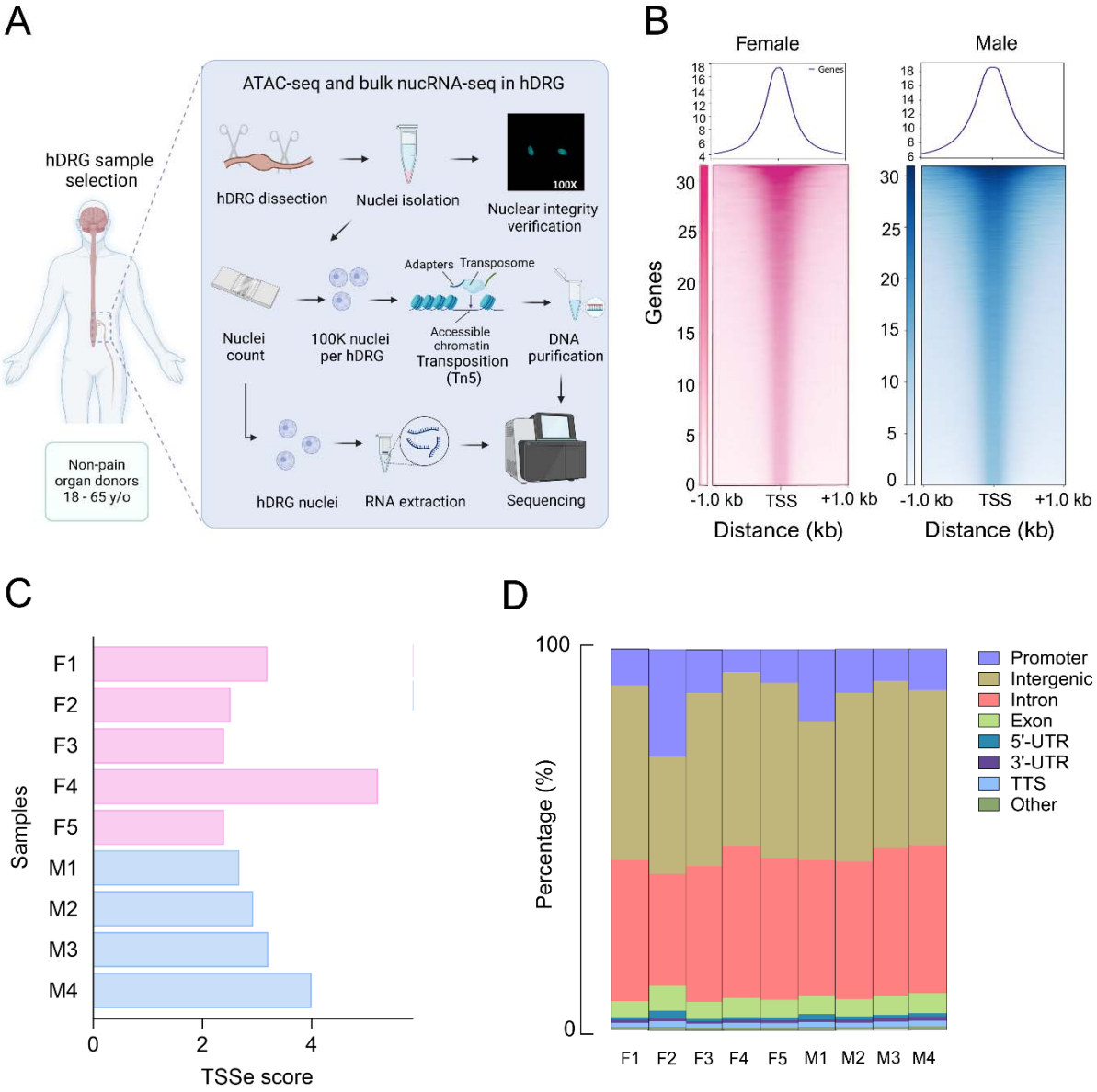

Figure 1. *Uncovering the open chromatin landscape in hDRG*. **A)** Schematic of the study design for bulk ATAC-seq. **B)** Heatmap shows chromatin accessibility around TSS ± 1 kb using aggregated peak enrichment scores from different female or male hDRG samples. Each row represents one consensus peak per gene spanning the TSS ordered by ATAC-seq signal intensity. Color represents the intensity of normalized chromatin accessibility. The metaplot on the top shows the mean ATAC-seq signal at the TSS. **C)** TSSe score obtained for each sample as a QC metric. **D)** Proportion of ATAC-seq peaks associated with different genomic annotations in each hDRG sample (UTR = untranslated region; TTS = Transcription Termination Site).

Sex differences in chromatin accessibility in hDRG

By comparing ATAC-seq peaks in female and male samples, we found 3005 differentially accessible chromatin regions (DARs, FDR < 0.01, **Fig 2A**), which were biased toward females in the total number of DARs (complete DAR list is supplied in **supp table 2**). Among these, 41 were identified in gene promoters in the female hDRG. Notably, the majority of DARs were located on the X chromosome in genes such as *NONO, MAPD7*, *FRMPD4, PORCN* and *FGF13* (**Fig. 2A**). In males, 234 DARs were associated with gene promoters (±1kb from TSS) on autosomal chromosomes and included genes such as *NR1D1*, *IRF2*, *ERBIN*, and *LIFR* (**Fig. 2A,** promoter DAR list is supplied in **Supp. table 3**). The ATAC-seq principal component analysis (**Fig. 2E**) demonstrated that female and male samples clustered separately, consistent with the DAR analysis results. Representative sex biased DARs around the TSS in female and male hDRG are shown in **Fig. 2C** and **D**, respectively. For our analysis we removed the Y chromosome but left the X chromosome because X inactivation can balance gene expression from this chromosome between sexes, although X inactivation is incomplete in many tissues and new regulatory functions associated with escape from X inactivation are still being discovered (42). We observed a striking number of DARs in this chromosome in the female DRG likely consistent with a lack of X silencing in the hDRG in females or the presence of poised genes ready to be activated. X inactivate-specific transcript (*XIST*), the long non-coding RNA (lncRNA) that primarily functions to silence one of the X chromosomes in each female cell, has been found to be dysregulated and participate in inflammatory and chronic pain in animal models (43-46), suggesting a possible X inactivation dysregulation which could become more relevant in pathological conditions.

To understand the epigenetic status of the Y chromosome in our samples, we conducted a supplementary analysis assessing chromatin accessibility differential peaks in the same samples, but this time we included the Y chromosome together with X and autosomes. As expected, this analysis identified Y-linked genes as DARs in males compared to females in hDRG (DAR list is supplied in **Supp. Table 4**). DARs in *DDX3Y*, *EIF1AY*, and *TMSB4Y* promoter were differential in male hDRG compared to

female (FDR < 0.01). Genes like *ZFY* and *UTY* had DARs in intronic, or intergenic regions. ATAC-seq signal for these genes is depicted in **Fig. S1A**. In line with this, all these genes were expressed at the RNA level in male hDRG samples (**Fig. S1B**). The total proportion of genes harbored in Y chromosome that was expressed in hDRG compared to the theoretical amount of protein coding genes in our experiments in hDRG was 17.77% (**Fig. S1C**). The function of these genes in pain or nociception has not been elucidated, but they have been associated with cellular functions such as transcription, translation, epigenetic mechanisms, and immune response (47).

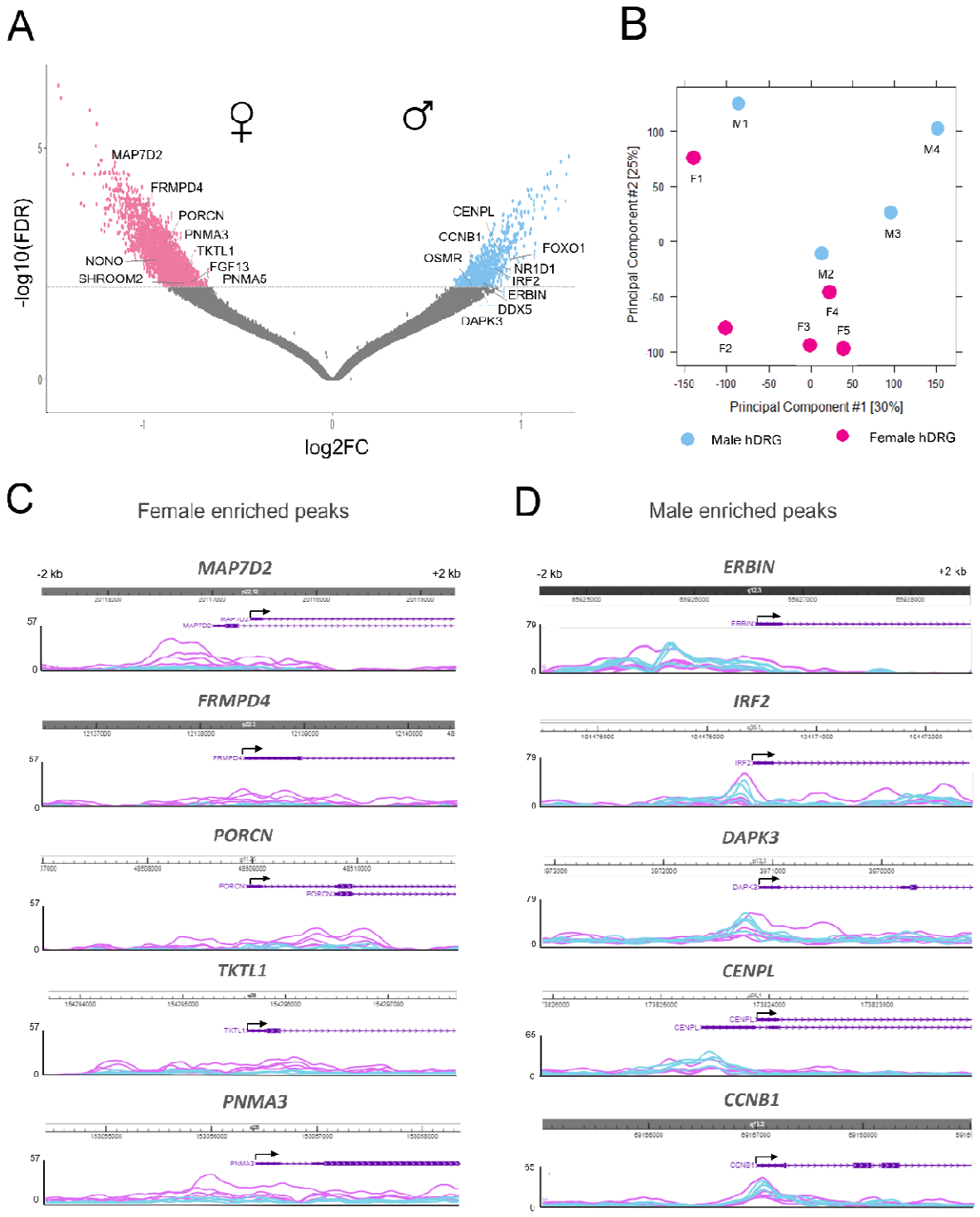

Figure 2. *Analysis of sex differences in open chromatin regions in hDRG*. **A)** Volcano plot showing DARs in hDRG between sexes (N = 9, 5 female (pink), and 4 male (blue) postmortem hDRGs, FDR < 0.01) identified with Diffbind. **B)** Principal component plot for ATAC-seq samples based on their similarity.

C) Genome browser views of ATAC-seq signal of DARs from female hDRG, all on the X chromosome. **D)** Representative genome tracks of DARs in male hDRG, all found in autosomes.

Enriched transcription factor binding sites in sex-biased DARs in hDRG

In addition to chromatin accessibility, ATAC-seq data enables the prediction of transcription factor binding to open chromatin regions. With the aim of dissecting sex-specific transcriptional activity programs in hDRG, we analyzed the differential transcription factor binding motifs within accessible chromatin regions between sexes in hDRG using Transcription factor Occupancy prediction By Investigation of ATAC-seq Signal (TOBIAS). For this analysis, differential binding scores with - log10 (p-value) larger than the 95th percentiles (top 5% in each direction) were considered as significant (48). We found a higher level of footprints for transcription factors that are part of the activating protein 1 (AP-1) family such as JUN, FOS, FOSL2, and ATF4 in males. In females, transcription factors of the EGR family such as EGR1 and EGR3, and members of the SP family such as SP1, SP2, SP4 and SP9 footprints were more abundant compared to male (**Fig. 3A-B**). Binding of transcription factors to the promoter of specific accessible genes was also an output of TOBIAS analysis. We found that the EGR1 transcription factor had open chromatin binding sites in *ADORA2B*, a synaptic-localized GPCR gene; *CX3CL1*, a chemokine known to participate in paclitaxel-induced macrophage recruitment in the DRG (49); and *JAK1*, a kinase essential for cytokine and growth factors signal transduction. EGR3 showed open chromatin binding sites in the promoter of *PIEZO2*, a mechanosensitive ion channel known for contributing to sensory neuron functions (50); *OXT, a* neuropeptide that suppresses action potential firing of DRG neurons (51, 52); *GLRA3*, a subunit of the glycine receptor; and *TACR1*, a substance P receptor. The promoter of SP1 had open chromatin binding sites for *TRPV2*, and inflammation-related genes such as *TRAF1/4*, *STAT4*, and *IKBKG*, and heat shock proteins like *HSF1*. Finally, SP4 showed open chromatin binding sites in Ca^{2+}-signaling-related genes such as *CACNA1G* and *CARHSP1*, as well as the interferon regulatory transcription factor, *IRF6*. Examples of genes predicted to be regulated by binding of EGR and/or SP transcription factors are depicted in **Fig. 3C**. AP-1 transcription factor and JDP2 binding sites in males had diverse common targets in the accessible chromatin in hDRG, mainly in cytokine-related genes including *OSMR*,

IFI16, *CCR7*, *NLRP3*, *TLR4* and *CASP8*. AP1 transcription factor binding sites were also found in GABAergic genes including *GABRA2* and *GABRB2* (**Fig. 3D**). Together, these results suggest that females and males have different transcriptional activation programs which could come play an important role in sex differences in response to injury.

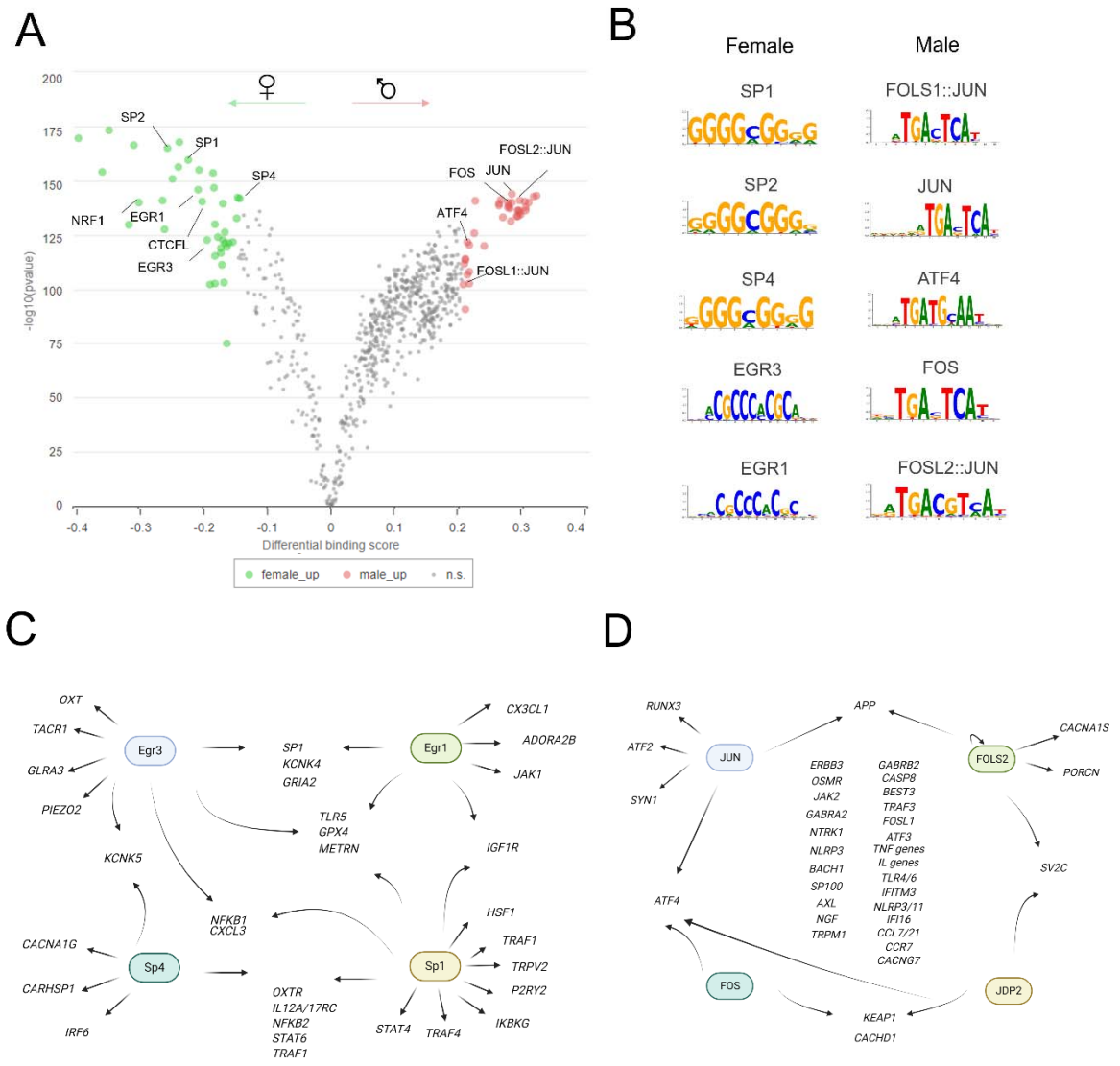

Figure 3. *Sex differences in transcription factor binding motifs within ATAC-seq peaks.* **A)** Volcano plot showing the differential transcription factor footprints enriched in female and male hDRG identified with BINDetect (N = 9, 4 male and 5 female postmortem hDRGs, -log10 (p-value)> 95th percentiles). **B)** Differential transcription factor consensus footprints in female and male hDRG defined by reference motif

on JASPAR repository. **C**) Genes predicted to bind EGR/SP factors due to transcription factor footprints in their promoters determined with TOBIAS. **D**) Genes with transcription factor binding sites for AP-1 factors in their promoters identified with TOBIAS.

Spatial ATAC-seq in hDRG

Since we did not perform neuronal selection for our bulk ATAC-seq experiments in hDRG, and spatial information is lost during dissociation, we used spatial ATAC-seq to dissect the chromatin profile in neuronal barcodes in a similar fashion to how we have done previously in spatial RNA-seq (17). We performed spatial ATAC-seq in hDRG tissue sections from 8 donors (N = 5 male, N =3 female) using a microfluidic barcoding system, followed by next generation sequencing (53).

We obtained 45,836 fragments on average in hDRG tissue, a TSSe score of 5.426 and a Frip of 0.1276 of fragments of reads in peaks (**Supp. Table 5**). The improved TSS score may be due to tissue preparation, since DRGs for spatial experiments were immediately frozen in the operating room while DRGs for bulk experiments were transported for 30-60 min in cold artificial cerebral spinal fluid (aCSF) prior to nuclear isolation (see **methods**). The average proportion of mitochondrial fragments was 4.15% (**Supp. Table 6**), and these reads were removed from the analysis. ATAC-seq fragment size distribution showed a typical periodicity of ~200 bp corresponding to reads, consistent with the length of DNA protected by mono-, di-nucleosomes (200, or 400 bp), as well as nucleosome free DNA (<100 bp) or open chromatin regions (**Fig. S2**), all of which is consistent with typical nucleosome packing (54).

In addition to neurons, there are at least 8 broadly defined cell types in hDRG (55-57). This high hDRG cellular heterogeneity was also observed at the epigenomic level, since unsupervised cell clustering in spatial ATAC-seq samples identified 9 groups of cells (**Fig. 4A**). Cluster 1 was classified as a neuronal cluster due to the abundance of chromatin accessibility in *SNAP25* gene compared to other cell types. Further, this cluster also shows chromatin activity for *CALCA* and *SCN10A* consistent with neuronal phenotype (**Fig. 4B-D**). Cluster 2 showed enriched chromatin accessibility for the marker of satellite glial cells (SGCs), *FABP7* (**Fig. 4E**). The chromatin accessibility profile for cluster 3 had *CD300LB, IFI30*, *C5AR1*, *C1QB* and *ABI3* in the top 30 active

genes, all of which are expressed by immune cells in the hDRG ((56) **Fig. 4F**). According to the hDRG harmonized atlas (56), the top 30 active genes for cluster 5 exhibited enrichment for immune-related genes, such as *OLR1*, *MS4A7*, *TYROBP* and *CORO1A*. Interestingly, this cluster also showed enrichment for macrophage markers such as *CD163, ARHGAP30, SIRPB2* and *PLCB2*. Thus, we classified cluster 5 as immune macrophage enriched (**Fig. 4G**). Cluster 6 showed enriched chromatin accessibility in *SCN7A* likely representing the non-myelinating Schwann cell cluster (**Fig. 4H**). Cluster 7 showed enriched chromatin accessibility in *PRX*, and *MPZ* representing the myelinating Schwann cell cluster (**Fig. 4I**) A Fibroblast cluster was identified by the gene activity of *DCN* and *FMOD* in cluster 8 (**Fig. 4J**). Cluster 9 was identified as the endothelial cluster due to abundant *CLDN5* gene accessibility (**Fig. 4K**). Cluster 4 was more challenging to classify. This cluster 4 showed chromatin accessibility in genes such as *PODN* and *FOXD1*, all of which are expressed in fibroblasts in hDRG suggesting this cluster is composed of a subtype of fibroblast in the hDRG. Cell type composition in hDRG section shows consistent cluster proportion between samples and sexes (**Fig. 4L**). The number of unique fragments per barcode exceeded the minimum values required to be considered high quality in all the clusters ($\log_{10}$ nFrag = 3, **Fig. 4M**). TSSe scores values per cluster and nucleosome ratio are depicted in **Fig. S3**. The number of final peaks identified across all donors was around 300,000 and the genomic annotation proportion was higher in intron and distal peaks, similar to our bulk ATAC-seq experiments (**Fig. 4N**).

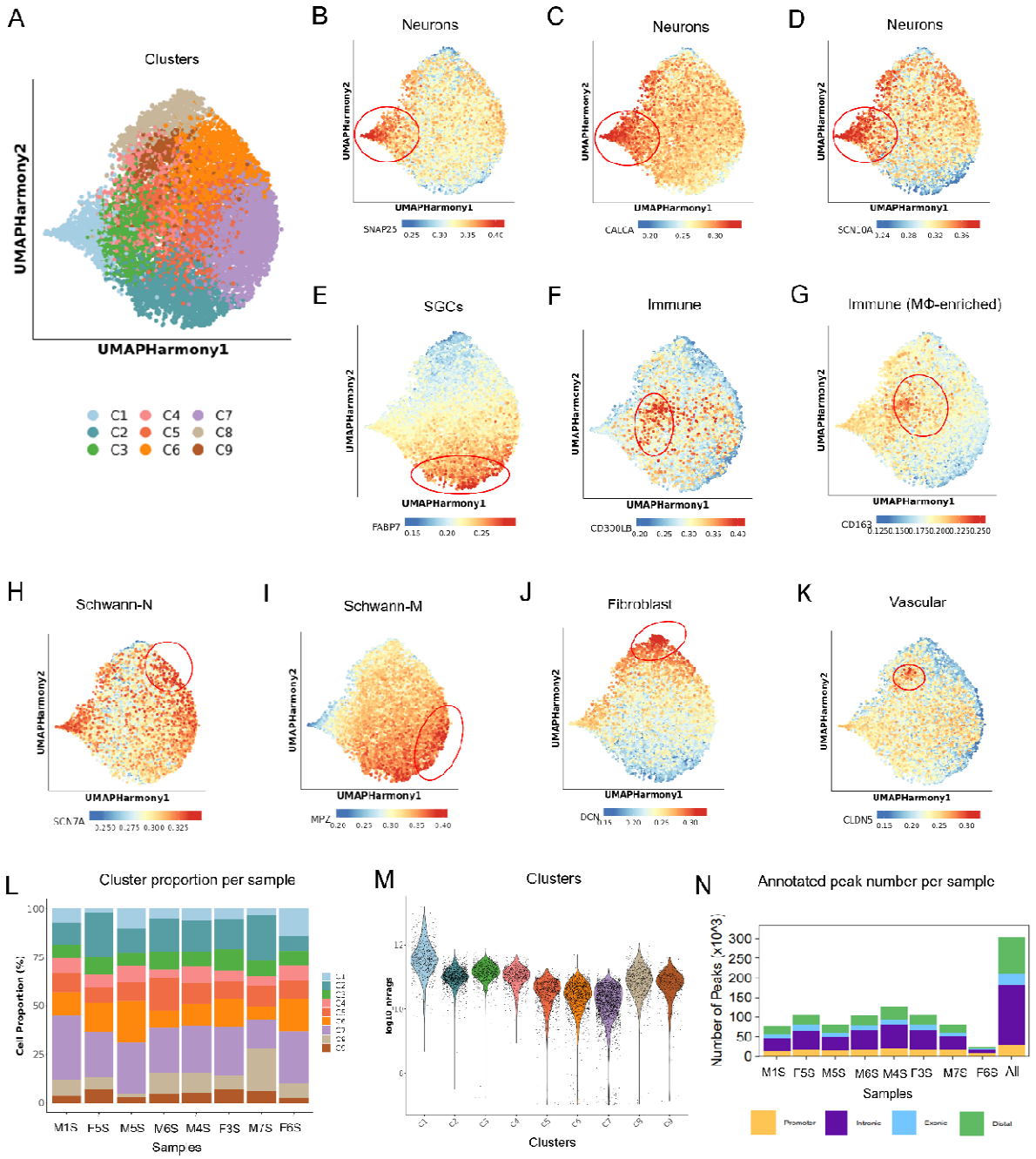

Figure 4. *Characteristics of spatial ATAC-seq in hDRG*. **A**) UMAP plot showing the 9 clusters generated by Seurat's workflow. **B-D**) UMAP plots of the chromatin accessibility of gene markers were used to label the neuronal cluster. **E-K**) UMAP plot showing cellular populations other than neurons, including satellite glial cells (**E**), immune cells (**F**), immune cells enriched in macrophages (**G**), Schwann-N cells (**H**), Schwann-M cells (**I**), fibroblasts (**J**) and vascular cells (**K**). **L**) Consistent cluster proportion in each

sample. **M**) Violin plot shows number of unique fragments per cluster. **N**) Number of peaks identified across all donors (all), and within samples associated and their genomic annotations: promoter, intron, exon and intergenic (N = 3 female, N =5 male; samples M5S, M6S, M7S and F6S belonged to donors whose samples had not been used before for bulk ATAC-seq. A frozen hDRG sample from donors M1, M4, F3 and F5 were used for spatial ATAC-seq, and are labeled as M1S, M4S, F3S and F5S).

Global sex differences in spatial ATAC-seq

We conducted a pseudo-bulk chromatin accessibility differential analysis between sexes using the reads from all the clusters in spatial ATAC-seq to have a general overview of sex differences in hDRG, which we hypothesized would be similar to our bulk ATAC-seq data (**Fig. 5**). In **figure 5A** we show that the number of fragments per barcode and the distribution of reads in the UMAP were similar between female and male hDRG samples (**Fig. 5B**). Our analysis showed DARs in 3796 gene promoters in females versus 3827 genes in male hDRG (**Fig. 5C**). In females, most of the DAR were, consistent with our bulk ATAC-seq finding, located on the X chromosome (**Fig. 5D**), with 98% of the genes in the top 500 DAR on the X chromosome. These findings corroborate our bulk ATAC-seq results indicating that the X chromosome is the primary driver of most of the observed DARs in females. Genes such as *NONO*, *MAPD7*, *FRMPD4*, *PORCN*, *FGF13* and *KTL1* shown in female bulk ATAC-seq were also found to be differentially accessible in female spatial ATAC-seq data. Spatial ATAC-seq also revealed female DARs in genes outside the X chromosome, such as *ERBB4*, GABAergic genes including *GABRG1/2*, *GABRA5*, *GABRB3*, *GABRB1*, *GABRA2/4*, and other neuronal genes such as *BDNF*, *RELN*, *KCNE5*, *SCN9A*, *GRIA4* and *GRIN2B*.

On the other hand, in males, the peaks spanned the whole genome with a higher abundance of DARs in genes located on chromosome 17 and 19 (**Fig. 5E**). We found male hDRG DAR-associated genes like *FOS*, *FOSL2*, *NR1D1*, *IRF2* and *FOXO1*. Interestingly, the male hDRG DAR list also included circadian related genes such as *BHLHE40* and *CSNK1D.* Cytokines such as *CSFR1*, *CCL2*, *IL4/6R*, and alarmins *HMGA1* were found to be more active in male hDRG. Hormonal associated genes such as *INSR* and *THRA* were also found to be epigenetically more active in males. Finally, DARs for epigenetic remodeler genes, such as *DOT1L*, *HDAC4*, *JARID2*, and *ARID1B/5B* were found in the male hDRG.

We also conducted transcription factor (TF) motif enrichment analysis to infer differential binding sites in spatial ATAC-seq data. In females, transcription factors such as TEAD1/4, NR3C1, and PGR were enriched in the spatial ATAC-seq dataset. In males, peaks in DARs again belonged to the AP-1 family such as FOSB, or AP-1 interacting factor like BACH1/2. (**Fig. 5F**)

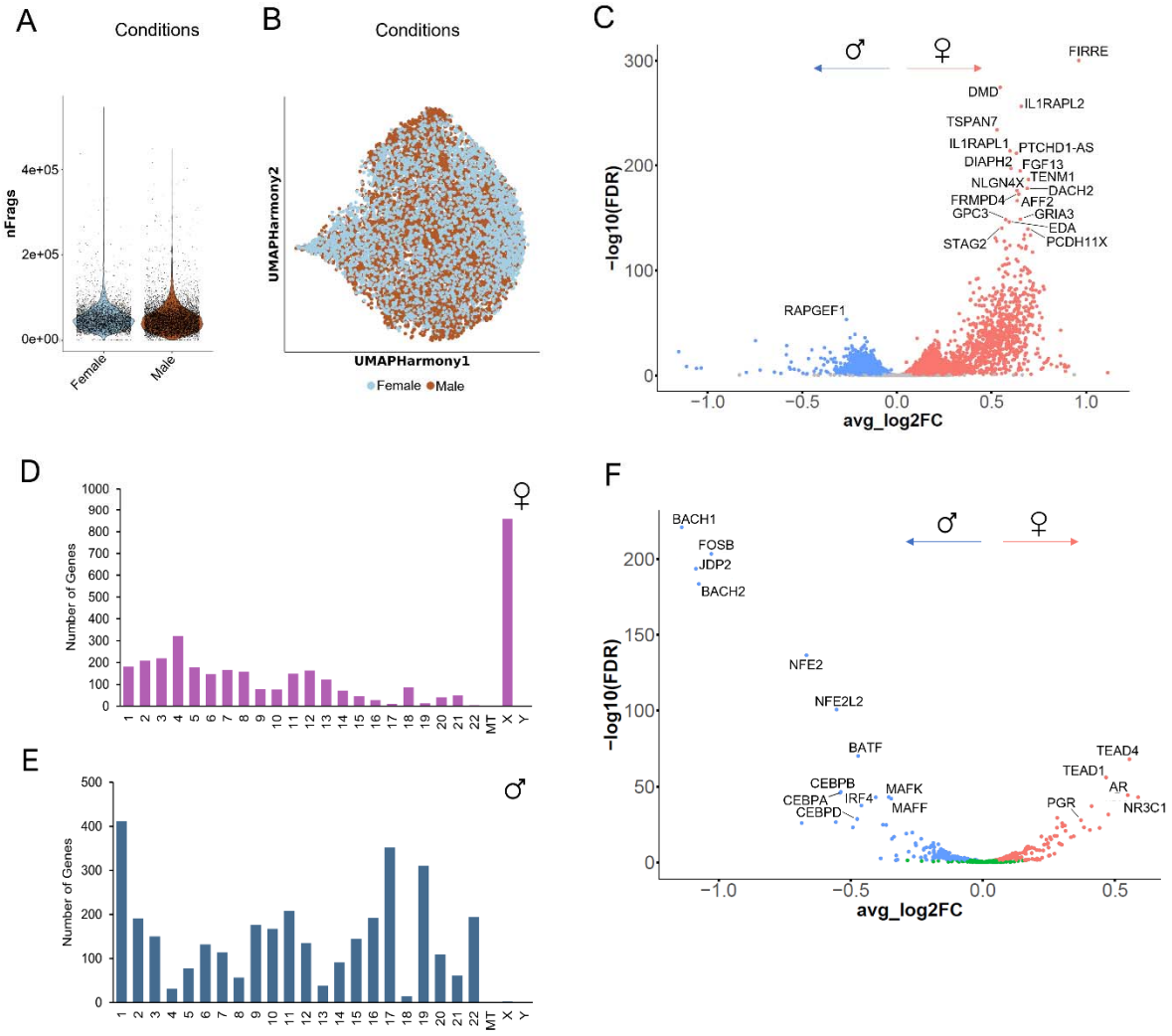

Fig. 5. *Differential spatial ATAC-seq signal in hDRG between sexes*. Analysis of sex differences in chromatin gene activity in hDRG. **A**) Number of fragments per barcode in female and male hDRG samples. **B**) UMAP of female and male barcodes distribution along hDRG cellular populations. **C**) Volcano plot showing differential ATAC-seq gene activity in a pseudo-bulk fashion in hDRG in female vs male (N = 4 female, 5 male postmortem hDRGs), FDR < 0.01 identified with ArchR. **D**) Genome location of DARs in female spatial ATAC-seq spanning the human chromosomes generated with ShinyGO. **E**)

Genomic position of DARs in male hDRG. **F**) Volcano plot showing differential transcription factor binding sites in female vs male hDRG (N = 4 female, 5 male postmortem hDRGs), FDR < 0.01 identified with ArchR.

Sex differences in chromatin accessibility in hDRG neurons determined with spatial ATAC-seq

A primary motivation of our spatial ATAC-seq approach was to identify potential sex differences in neurons in hDRG. To examine this, we compared chromatin accessibility in the neuronal-enriched cluster between sexes (**Fig. 6**). DESeq2 analysis revealed DARs associated with 1665 genes in females and 1089 genes in males ($p_{adj} < 0.01$, **Fig. 6A**). Similar to what we observed previously with bulk ATAC-seq or the global changes in spatial ATAC-seq, most of the peaks in females were located on the X chromosome ($p_{adj} < 0.01$, 643 out of 1665 genes, **Fig. 6B**). In male neurons, the genes were distributed across the entire genome, and again, there was a higher abundance observed on chromosome 17 and 19 (**Fig. 6C**).

The analysis of gene ontology of genes associated to DARs between sexes showed that glutamatergic genes such as *GRIA2, GRIA3,* and *GRIA4* to be found in the top 100 DARs in female hDRG chromatin. GABAergic genes such as *GABRB1*, *GABRG1*, *GABRE*, *GABRQ*, *GABRA1/2/3/6* were also DARs in female hDRG within the differential female gene-set, together with the lncRNA *BDNF-AS*. Enrichment analysis of accessible regions showed an association between open chromatin regions and glutamate receptor activity as the main gene ontology enriched molecular function category (pval: 0.00001581, **Fig. 6D**) determined with EnrichR (58). Interestingly, neurons in female donors also showed DARs in *ACE2*, some interferon related genes such as *IFNB1*, *IFNA5/8/17*, *IFIH1*, *IFI44* and *CASP1/4*. Centromere genes such as *CENPE/I/W* were DARs in female compared to males.

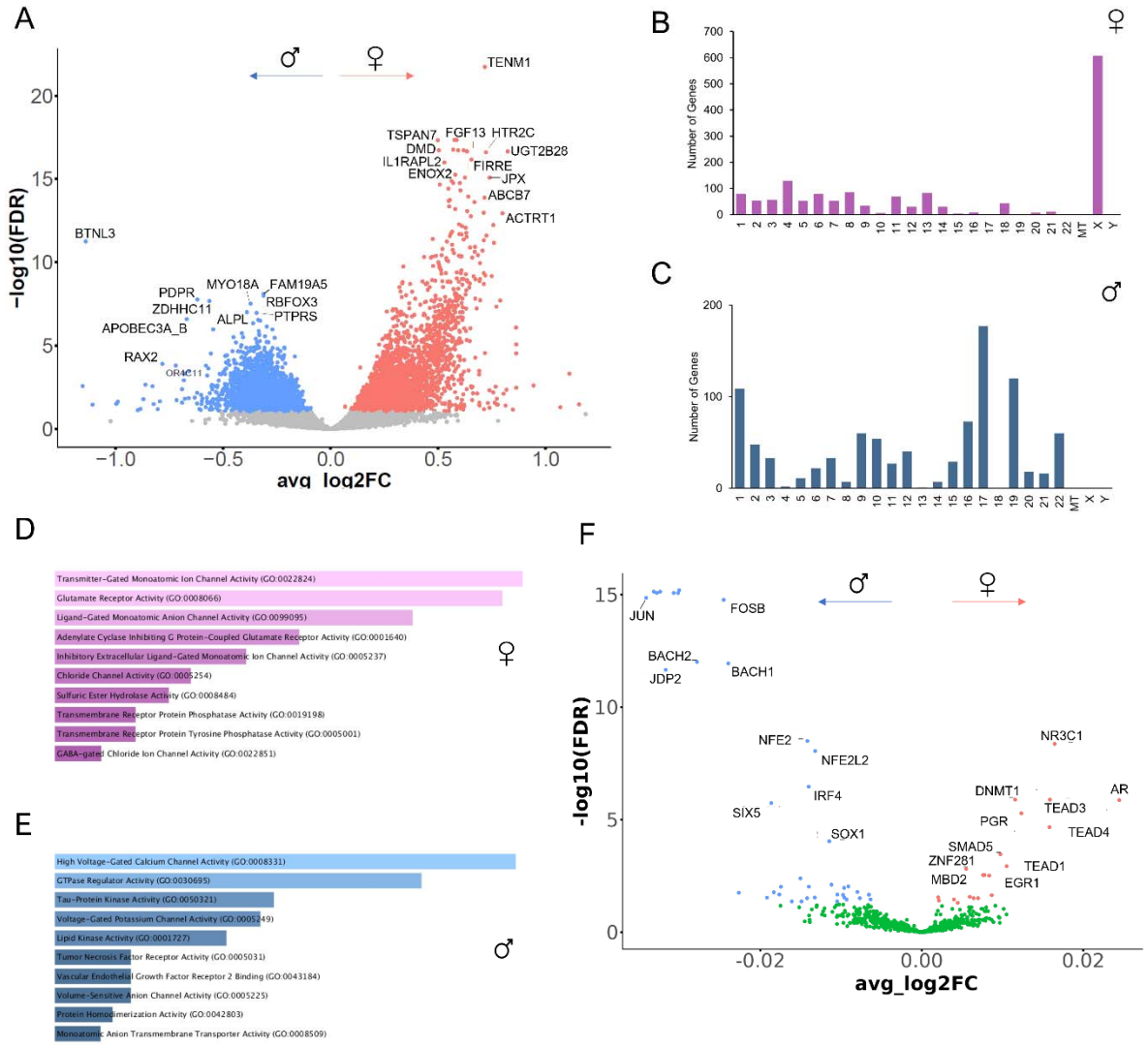

Fig. 6. *Sex differences in spatial ATAC-seq DARs in the neuronal cluster*. **A**) Volcano plot showing DARs in spatial ATAC-seq neuronal clusters in hDRG neurons in female vs male (N = 4 female, 5 male postmortem hDRGs, FDR < 0.01 identified with ArchR. **B**) Genome location of DARs in female neuronal ATAC-seq spanning the human chromosomes generated with ShinyGO. **C**) Genomic position of the DAR gene set in males. **D**) Overview of the molecular function gene ontology for DAR-associated genes in female neurons in hDRG. **E**) Summary of the gene ontology related to molecular functions for DAR-associated genes in male neurons in hDRG. **F**) Volcano plot showing transcription factor binding site enrichment in DARs in hDRG neurons in females vs males (N = 4 female, 5 male hDRGs), FDR < 0.01 identified with ArchR.

In male neurons, genes such as *CACNA1B*, *GRIK3*, and *PTPRS* were found in the top 100 DARs. Voltage-gated Ca^{2+} channel related genes such as *CACNA1C, CACNA1D*,

and *CACNA1H* were found in the male DAR gene set. Interestingly, *TRPV1/3/4* were also DARs in males compared to female neurons. Gene ontology analysis of the male DAR gene set revealed high abundance of calcium channel activity in the molecular function category (p_{val} = 0.00165, **Fig. 6E**). Gene ontology analysis for the other clusters can be found in **Fig. S4**.

Finally, we analyzed the neuronal cluster for enrichment of transcription factor binding sites in the DARs between females and males (**Fig. 6F**). In females, transcription factors such as *EGR1*, *TEAD1/3/4*, *NR3C1* and *PGR* were enriched. We again found AP-1 family transcription factor enrichment in males including *JUN*, *FOSB*, *BACH1/2* and *IRF4* (**Fig. 6F**).

Patterns of chromatin accessibility in hDRG are moderately positively correlated to the transcriptomic profile.

In light of the sex dimorphic differences in chromatin accessibility between sexes in our bulk ATAC-seq results, our next approach entailed conducting a differential gene expression analysis on bulk ATAC and nuclear RNA-seq (nucRNA-seq) paired samples. RNA extractions and sequencing was performed in nuclei extracted from DRGs of 7 donors (N=3 females, N=4 males (same set of participants as in bulk ATAC-seq; details in **Supp. Table 1**). We found only 8 genes that were statistically different between sexes (p_{adj}<0.05, fold change >1.33, **Supp. Table 7**). Females showed higher expression of chemokine genes such as *CCL3* and *CCL4*. On the other hand, males showed higher gene expression of non-coding genes such as *KDM5DP1*. An interesting point to highlight is that *EGR1* and *EGR3* were trending to be highly expressed in females compared to males in our RNA-seq data (**Fig. S4A**), which aligns well with transcription factor footprints in our female ATAC-seq data sets. Although we did not find a large number of differentially regulated genes between sexes, our data harbors information about the RNAs that are transcribed and about other types of RNA that remain in the nuclear space. Around 30% of the RNAs were lncRNAs, 40% were protein coding, and the rest were other types of RNA in both female and male hDRG (**Fig. S4B**). The high abundance of lncRNAs in the nuclear compartment is pivotal for their interaction with nucleic acids and RNA-binding proteins. They participate in gene

expression modulation and chromatin remodeling by engaging with key chromatin-modifying proteins (59). LncRNAs achieve this by forming complexes with transcription factors, loops of DNA, and histones. Their expression is tissue-specific, with the nervous system being notably enriched in these RNAs (60). As expected among the lncRNAs in females, we found *XIST*.

We tested the correlation between the log2 fold change in DARs situated in promoter and within gene bodies (39), including exon, and intron regions in ATAC-seq and the log2 fold change in nucRNA-seq for those genes in the matched hDRG samples. We found a weak positive correlation between the transcriptional profiling and the chromatin accessibility (**Fig. S4C**). This weak correlation could be explained by the repertoire of RNAs analyzed, which were limited to nuclear space and not to the whole cell. Evidence has shown that nuclear compartment harbors abundant lncRNAs and small nucleolar RNAs in human brain tissue, consistent with our nucRNA-seq results, while the cytoplasm contains RNAs associated to cellular function such as metabolism, translation and protein organization compared to the nuclear compartment (61). In addition to the small sample size, another explanation is that a high correlation is not typically observed since accessible regions are not necessarily associated with actively transcribed genes, or they are associated with genes that are poised to become active under specific conditions (38). Consistent with this logic, we observed that genes on the X chromosome exhibit a median to low level of expression. Six out of 41 DARs in gene promoters in X chromosome had medium expression in nucRNA-seq (14.6%, TPM (Transcripts Per Million) >10 up to 80), including *MAP7D2*, *PORCN*, *PNMA3*, *CHRDL1*, *NONO* and *FGF13*, while 13 out of 41 had low expression (26.8%, TPM < 10) (**Fig. S4D**). The rest of the genes did not show gene expression (58.6%). In males, 142 out of 234 DARs in gene promoters showed medium expression (56.1%), and 31 had low expression (12.3%). Eighty DAR-associated genes (31.6%) were not expressed in male hDRG (**Fig. S4E**). It is important to denote that transitions in the deposition of histone modifications as well as transcription factor binding to regulatory sites such as enhancers can precede gene expression changes, inducing poised or primed chromatin states (62), which are indistinguishable from active chromatin in ATAC-seq due to a lack of epigenomic context. Further research combining different histone and DNA

modifications is required to better understand the epigenomic landscape and to get a better interpretation and understanding of gene regulation in this complex tissue.

EGR1 expression in hDRG

One of the outcomes that showed consistency in bulk and spatial ATAC-seq was the bias toward female in the footprint scores for the transcription factor EGR1 in hDRG. We found a trending coincidence at the gene expression level in bulk RNA-seq. With the aim of validating this consistent finding we sought to assess the expression of *EGR1* in hDRG using *in situ* hybridization. We found that *EGR1* is expressed in female and male hDRG *SCN10A* (+) and (-) neurons, but also in cells surrounding neurons, likely satellite glial or immune cells (**Fig. 8A-B**). We quantified the number of *EGR1* mRNAs localized to hDRG neurons and found it more abundant in female compared to male (**Fig. 8C**). This sexual dimorphism was statistically significant in *SCN10A* (+), but not *SCN10A* (-) cells in females (**Fig. 8D-E**). Our analysis also showed that females have a higher number of *EGR1* (+) *SCN10A* (+) cells compared to males (57.9% vs 29.71%, respectively, **Fig. 8F**). These results are consistent with our data sets. The combined identification of EGR1 female-biased expression and the prominent abundance of regulatory binding sites in female hDRG, renders the transcriptional activity of EGR1 a strong candidate for a female-biased regulator of gene expression in hDRG neurons.

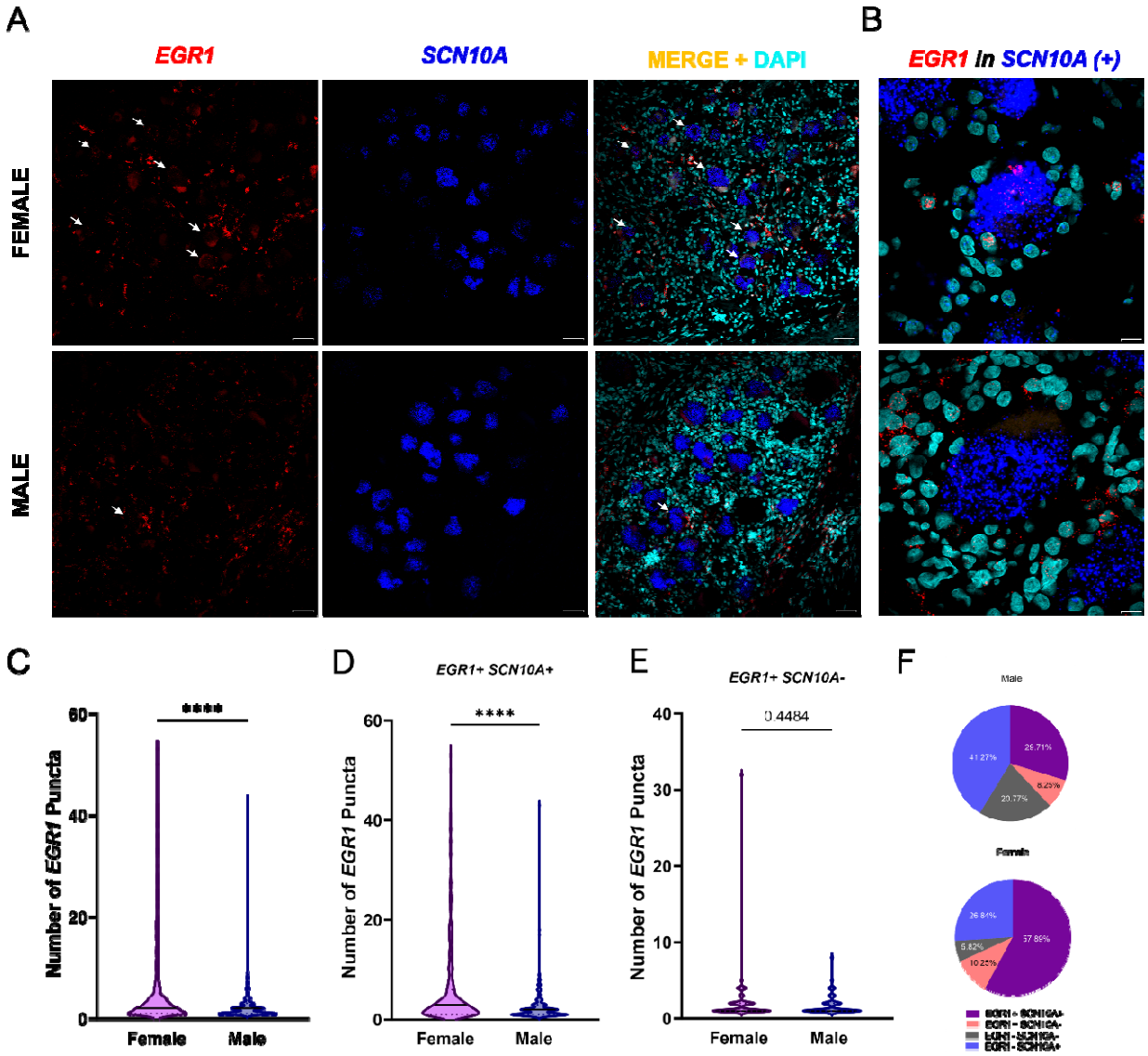

Fig. 8. *EGR1* is expressed in more *SCN10A* positive neurons in females compared to males in hDRG. **A)**. Representative *in situ* hybridization images of *EGR1* (red) in *SCN10A* (+) neurons (blue) in female and male hDRG. *EGR1* positive neurons are indicated with an arrow. **B**) 100 X magnification of neurons with *EGR1* mRNAs in female and male neurons. **C**) Total number of *EGR1* mRNAs in neurons. **D-E)** Number of *EGR1* mRNAs in *SCN10A* positive and negative neurons, respectively. **F)** Percentage of *EGR1* positive cells in *SCN10A* positive or negative cells across female and male donors in hDRG. A total of 722 neurons were analyzed to assess *EGR1* expression in female hDRG, and 727 in males (N = 5 female, N = 5 male DRG). Data are presented as violin plots with thick line indicating the median and the dotted lines indicating the quartiles. Section thickness – 20 µm. Scale bar – 50 µm for **A** and 10 µm for **B**. ****p<0.0001 as determined by t test in **C-E**.

Discussion

Our work provides a comprehensive view of the chromatin accessibility profile in hDRG and focuses on sex differences in tissues recovered from organ donors without any history of chronic pain or neuropathy. Chromatin structure plays a crucial role in transcription through the control of the access to regulatory factors in DNA. We mapped the accessible genome in hDRG using two different approaches, bulk ATAC-seq and spatial ATAC-seq. The latter approach resolved hDRG chromatin accessible profiles in distinct cell types where we focused on neuronal signatures. Our work shows a profound sexual dimorphism at the chromatin level between sexes in hDRG from non-pain organ donors. This dimorphism is mainly driven by the X chromosome in female hDRG suggesting a reduced X inactivation or a dormant transcriptional state that can readily become activated under certain circumstances. Second, our ATAC-seq data show a sex dimorphic signature in transcription factor bindings sites in accessible chromatin. EGR and SP transcription factor families binding sites were more prominent in female hDRG open chromatin while accessible chromatin in males was enriched for motifs that can be regulated by transcription factors such as AP-1 and IRF families.

Finally, our work shows sex differences in neuronal chromatin accessibility using spatial ATAC-seq. In neurons, sex differences were again mainly driven by the X chromosome in females but using this approach we also uncovered differences in genes located in autosomes. GABA-A channels and glutamatergic genes were the molecular ontologies associated with accessible DNA in females, while in male hDRG, voltage gated Ca^{2+} and K^{+} channel genes as well as GTP associated proteins were associated with accessible chromatin.

Our findings point to a striking sexual dimorphism at the chromatin level shaped by the X chromosome. Most of the DARs in bulk ATAC-seq data mapped to X chromosome in females. Independently, spatial ATAC-seq also confirmed this finding. It is known that one of the two X chromosomes in females is epigenetically silenced to compensate for the imbalance of X dosage between the female and male genome (63). X inactivation is triggered by the upregulation of *XIST* early in development. XIST coats one of the X chromosomes in *cis* (64, 65) inducing X heterochromatization via a repressive

epigenetic signature (66). Interestingly, a subgroup of genes, comprising 8-15% of the genes in X, escapes inactivation and these genes are characterized by epigenetic marks of active transcription, allowing gene expression from the inactive X (Xi) chromosome (67). Our findings show that *XIST* RNA is differentially expressed and there are more DARs associated with this gene in the adult female DRG. This finding is consistent with previous observations in the adult human tibial nerve (68). It is also consistent with a very recent study showing greater variability in X inactivation in excitatory neurons in the human brain suggesting enhanced expression from this chromosome in women in this population of neurons that shares a glutamatergic biochemical phenotype with DRG neurons (69).

It is now recognized that sex dimorphisms in pathological conditions, like autoimmune diseases, can be driven by tissue or cell-specific patterns of X-inactivation. We observed higher chromatin accessibility mainly in genes coding for GABA-A receptor subunits, glutamatergic and interferon-related genes in females, many of which are located in X chromosome. For X chromosome genes, we observed that several interferon signaling-related genes and *ACE2* are highly accessible in female hDRG neurons. This is in line with previous findings showing that the interferon-related genes are more highly expressed in female than in male DRG from neuropathic pain patients undergoing thoracic vertebrectomy surgery (14). Moreover, it has been shown that *ACE2* is expressed in hDRG neurons, serving as potential entry site for SARS-CoV-2 in the PNS (70). Delving deeper into the study of X inactivation escape in hDRG will shed light on the organization of chromatin on this chromosome and improve our understanding of its implications for chronic pain mechanisms in women. Importantly, a previous study linked X inactivation escape in blood cells to development of chronic pain after motor vehicle accident-related injury supporting the relevance of this line of investigation (71). Some of these genes were associated with DARs on autosomes, like *GABRA5*. Previous studies have shown that the alpha-5 GABAergic receptor (encoded by the *Gabra5* gene in mice) is more highly expressed in the female rodent DRG where it plays an important role in pain signaling and where it is epigenetically regulated in a sex-specific fashion (72, 73). We also found a higher accessibility in autosomal *BDNF-AS* in females, a lncRNA that suppresses *BDNF* expression. It is well-established that

BDNF is released from primary afferents (74) binding to TrkB in spinal cord neurons where it regulates synaptic plasticity important for chronic pain (75). Our findings suggest that *BDNF-AS* could be an unappreciated suppressor of BDNF expression in females, a relevant finding because other studies have shown a more prominent role for BDNF signaling in male than in female rodents (76, 77) and in male but not female human spinal cord (78).

At the level of transcription factor footprints, EGR1/3 and SP transcription factors showed higher abundance in female accessible DNA in hDRG. In agreement with this, *EGR1* expression was biased to females in our RNA-seq results. EGR1 is a transcription factor classified as immediate early gene. EGR1-driven transcriptional programs are activated by stimuli like cytokines, growth factors, oxidative stress, hypoxia and tissue injury (79). Further, Egr1 has an important role in neuronal plasticity in the adult nervous system (80). A recent study found that *Egr1* expression is driven by female sex hormones and acts as a chromatin modifier in a sex-dependent manner (81), suggesting a pivotal role of this transcription factor in controlling neuronal gene expression in females. Our data shows that EGR1 binding sites are found in genes like *JAK1* and *CX3CL1*, both of which are interferon signaling pathway associated genes that are known to induce pain through a peripheral mechanism in mouse models (82, 83). This is also consistent with human thoracic vertebrectomy DRG data showing that interferon and JAK-STAT signaling are associated with neuropathic pain in female samples but not in males (14). One inconsistency with the thoracic vertebrectomy data is that *EGR1* mRNA was more highly expressed in males with pain than females (14), but the impact of that difference likely depends on access to regulatory sites for the transcription factor. Also consistent with our findings, *SP4* has been shown to have a higher expression in female tibial nerve compared to male (15). Like EGR1, SP4 regulates the transcription of pain-related genes (25) and, it has been described the reversal of hypersensitivity due to Sp4 knockdown in persistent models of pain in mice, suggesting an important role of this transcription factor to pain (84). Since, we observed other members of the SP (*SP1*/*SP5*) family with binding sites in DARs in female DNA in hDRG, this family of transcription factors may be an important potential therapeutic

target for treating pain in females since it is linked to neuropathies such as of chemotherapy-induced peripheral neuropathy (85).

In males, we observed a higher chromatin accessibility in *TRPV* and Ca^{2+}-related genes in neurons. With respect to the former group of genes, many of these play important roles in pain but *TRPV4* is the only TRP channel that shows higher expression in pain samples from thoracic vertebrectomy pain patients in males versus females (14). While we are not aware of any previous reports of sex difference in expression of Ca^{2+}-related genes in hDRG, rodent studies demonstrate that Ca^{2+}-related genes such as *Cacng8, Cacna1a/b* and *Cacng4/5* are upregulated in male DRG in a model of nerve injury (86), genes that had higher chromatin accessibility in our male hDRG data. At the level of transcriptional programs, AP-1 transcription factors were predominant in accessible chromatin in male compared to female in both bulk ATAC-seq and spatial ATAC-seq specifically in neurons. These data are in close agreement with increased JUN and FOS activated transcriptional cascades in DRGs from male patients with neuropathic pain in the thoracic vertebrectomy cohort (14). Our transcription factor footprint analysis data showed that promoters of genes such as *OSMR*, *NLRP3* or *CASP8* are predicted to be bound by these transcription factors. The abundance of binding sites for these genes in male open chromatin in the DRG increases the likelihood that they will be activated under conditions of inflammation or injury, which is again consistent with the findings of the thoracic vertebrectomy cohort where OSM signaling was specifically upregulated in males (13, 14).

Collectively, our data using bulk ATAC-seq and spatial ATAC-seq demonstrate distinct baseline chromatin accessibility patterns between female and male hDRG. These patterns suggest sex-specific transcriptional programs primed for activation by injury or inflammation. Functional differences observed in female hDRG, such as increased accessibility of GABAergic, glutamatergic, and interferon-related genes, could contribute to their heightened susceptibility to chronic pain. Conversely, higher accessibility of calcium signaling genes in males might underlie distinct pain mechanisms. These findings highlight the importance of considering sex as a biological variable in chronic

pain research and potentially pave the way for the development of sex-specific therapeutic strategies.

Limitations

This study has several limitations. The most obvious one is that we did not do multi-omics from the same cell, making it difficult to test for direct correlation of gene expression and chromatin accessibility. Another potential limitation is the relatively small sample size. This can be improved with additional studies, studies which should also include samples from individuals with chronic pain conditions. We note, however, that we could achieve our primary objective of detecting sex differences even with the relatively small sample size and many of these were replicated with two independent methods. ATAC-seq is not the only method that can be used to assess the epigenetic landscape of a tissue. Additional methods like CUT&Tag sequencing (87) can be used in the future to gain insight into epigenetic marks in the hDRG. Our work with organ donor DRGs shows that tissue quality is of sufficient quality to enable these future studies.

Methods

DRG tissue preparation

All human tissue procurement procedures were approved by the Institutional Review Board at the University of Texas at Dallas. Lumbar DRGs from human organ donors were obtained via a collaborative effort with the Southwest Transplant Alliance. Right after dissection, human L4 or L5 DRGs from male and female organ donors were either transported in aCSF to be further processed within our facilities or frozen in dry ice right after dissection and stored in a −80 °C freezer. DRG donor demographic information is provided in **Supp. Table 1**. The inclusion criteria for this study took into account adult donors aged 18 to 65 years who exhibited no signs of pain or neuropathy. The cutoff age of 65 years old was determined based on prior epigenomic studies, which indicated significant alterations in both males and females occurring notably after the age of 65 (88).

Bulk ATAC-seq on fresh hDRG

Immediately after dissection, human L4 or L5 DRGs from male and female organ donors were transported in cold bubbled NMDG-aCSF pH 7.4 (93 mM NMDG, 2.5 mM KCl, 1.25 mM NaH_2PO_4, 30 mM $NaHCO_3$, 20 mM HEPES, 25 mM glucose, 5 mM ascorbic acid, 2 mM thiourea, 3 mM sodium pyruvate, 10 mM Mg_2SO_4, 0.5 mM $CaCl_2$, 12 mM N-acetylcysteine; osmolarity 310 mOsm (89) in ice to our facilities. Using scissors, tissue was chopped in 2 mL of ice-cold nuclei isolation buffer (90). This buffer contained: 250 mM sucrose, 25 mM KCl, 5 mM $MgCl_2$, 10 mM Tris-HCl pH 8.0 and 0.1% triton X-100. The total volume was transferred to a Dounce homogenizer. 5 strokes of the loose pestle and 15 strokes of the tight pestle were applied. The homogenate was transferred to a conical tube and centrifuged at 100 x g for 8 min at 4 °C. The supernatant was carefully removed without disrupting the soft pellet. Next, the tissue was resuspended in a 2 mL nuclei isolation buffer free of triton. The supernatant was removed without disrupting the pellet after centrifugation at 100 x g for 8 min at 4 °C. Subsequently, the nuclei were resuspended in a 2 mL nuclei isolation buffer without triton and filtered through a 40-um cell strainer. The number of isolated nuclei was counted using a hematocytometer. A total of 100,000 nuclei were aliquoted and

centrifuged at 500 x g for 10 min at 4 °C. The supernatant was then removed, and the pellet was utilized for the tagmentation reaction and DNA purification using the Active Motif kit (Cat. No. 53150). In brief, 50 uL of Tagmentation Master Mix (consisting of 2X Tagmentation buffer, 10X PBS, 0.5% digitonin, 10% tween 20, and assembled transposomes) was added to each sample. The tagmentation reaction was incubated at 37 °C for 30 min in a thermomixer at 800 rpm. Subsequently, 250 uL of purification binding buffer and 5 uL of 3 M sodium acetate were added. DNA purification columns were employed to isolate the DNA, and the tagmented DNA was eluted in 35 uL of DNA elution buffer. The amplification of tagmented DNA through PCR was carried out using i7- and i5-Illumina's Nextera-based adapters as per the provider's instructions. Pair-end 75 cycle sequencing reads were acquired on the Nextera500 sequencer or Nextera2000 sequencer. A total of 100 million reads were obtained from each sample.

RNA-seq on fresh hDRG

After isolating 100,000 nuclei from hDRG for bulk ATAC-seq, the remaining extracted nuclei were used to perform RNA extraction with the aim of sequencing and pairing bulk nucRNA-seq with ATAC-seq from the same sample. Four male and 3 female hDRG samples were utilized to extract RNA, thus the pairing with ATAC-seq samples was performed in 6 out of 10 ATAC-seq samples.

Total RNA from hDRG nuclei was purified using TRIzol™. RNA peak profiles were analyzed using 5200 Fragment Analyzer and quantified with Qubit. RNA quality number was used to assess RNA Integrity (**Supp. Table 8**). Illumina Tru-seq stranded RNA library prep was used to generate cDNA libraries according to the manufacturer's instructions. Next Generation Sequencing (RNA-seq) was performed in a NextSeq 2000 sequencer. Single-end sequencing was performed in a multiplexed fashion by loading the samples on a P2 flow cell, averaging ~50 million reads per sample.

Spatial ATAC-seq on frozen hDRG

The frozen hDRGs were gradually embedded in OCT in a cryomold by adding small volumes of OCT over dry ice to avoid thawing. A total of 8 hDRGs were used for these experiments (N=3 female, N=5 male) and demographic information of the organ donors

is provided in **Supp. Table 9**. All tissues were cryostat sectioned at 10 µm onto SuperFrost Plus charged slides (Fisher Scientific; Cat 12–550-15). Sections were only briefly thawed in order to adhere to the slide but were immediately returned to the −20 °C cryostat chamber until completion of sectioning. The slides were removed from the cryostat and sent to AtlasXomics for further processing (53). Spatial ATAC-seq (AXO-0303) consisted of the next steps: The tissue was fixed for 5 min with 0.2% paraformaldehyde. Afterwards, the tissue was treated with glycine and left to dry. Then, a tissue permeabilization step was performed using 0.2% NP40 for 15 minutes. Tn5 transposition on the fixed hDRG sections was carried out for 30 min. Adapters containing a ligation linker were added to the preparation to be inserted in accessible genomic loci. Barcodes with linkers were introduced using microchannels and were ligated to the 5′ end of the Tn5 oligo through successive rounds of ligation. hDRG sections were imaged to correlate spatially barcoded accessible chromatin with tissue morphology. A barcoded-tissue mosaic was created, reverse cross-linking was performed to release DNA-fragment, which were then amplified through PCR for subsequent library preparation. 150X150 paired-end sequencing was performed using NextSeq 2000 with 15% PhiX. Sequencing depth was up to 300 million reads per sample.

Processing of ATAC-seq data

First, we verified the quality of raw sequencing fastq files using FastQC v0.11.7. We removed adapters using TrimGalore-0.6.6 and verified the quality of trimming using FastQC v0.11.7. Paired-end reads were mapped to the reference genome GRCh38/hg38 using Bowtie2. To remove unmapped reads, low quality reads or reads that mapped to mitochondrial DNA and PCR duplicates we used Bamtools. Areas of open chromatin were identified by peak calling for each sample using Macs2 v.2.2.7.1 in keeping with Galaxy ATAC-seq data analysis. Differential accessibility between male and female donors was detected using DiffBind, a package within the Bioconductor framework. Next, we used HOMER annotatePeaks which uses the program assignGenomeAnnotation to efficiently assign ATAC-seq peaks to a genomic annotation. The definitions of annotations were acquired in a default mode. Processing

of transcription factor binding sites was performed using Transcription factor Occupancy prediction By Investigation of ATAC-seq Signal (TOBIAS, (48)) in conjunction with human consensus transcription factor motifs from JASPAR. In brief, ATACorrect parameter was used to assess and correct the Tn5 transposase sequence preference of cutting sites. Putative transcription factor binding sites or transcription factor occupancy within peak regions were estimated using FootprintScore. Differential transcription factor binding sites in ATAC-seq reads between male and female hDRG were detected with BINDetect. Differentially Accessible Regions (DARs) were identified using DESeq2 v1.42.0.

Processing of RNA-seq data

We confirmed the quality of raw sequencing fastq files using FastQC v0.11.7. The STAR alignment tool (v2.7.10b) was employed for aligning sequenced reads to the human GENCODE reference genome (v38). Sequenced reads underwent trimming to reduce sequencing quality issues at both ends. Relative abundance quantified as TPM was generated using the Stringtie tool and HTseq for counts generation.

Processing of spatial ATAC-seq

Processing of spatial ATAC-seq was performed as done previously by others (53). Chromap was used to perform the alignment of sequenced reads to the human GENCODE reference genome (v38) and remove duplicates from fastq files (91). Fragments files containing coordinates of sequenced DNA molecules mapping to barcodes were generated for downstream analysis. For data visualization, pixels on tissue samples were designated using AtlasXbrowser based on microscopy images to create Seurat-compatible metadata files. ArchR was used to process fragments files and the remotion of pixels not on tissue were removed. Data normalization and dimensionality reduction was applied to the data using ArchR's iterative latent semantic indexing and subsequent graph clustering and Uniform Manifold Approximation and Projection (UMAP) embedding were performed. ArchR functions were used to acquire gene accessibility scores and matrices (gene score model), marker genes for clustering, and genome browser tracks. ShinyGO-080 was used to plot chromosomal location of DARs-associated genes to the human genome.

In situ hybridization

hDRGs from non-pain donors (N=5 males and N=5 females) were embedded in OCT using a cryomold over dry ice and sectioned in 20 µm thickness. Donor information for these experiments is provided in **supp. Table 5**. Slices were placed onto SuperFrost® Plus charged slides (Thermo Fisher Scientific, cat. No. 1255015). Two sections per hDRG separated by at least 100 µm from each other were obtained to capture two sets of neurons allowing for a diverse population to be analyzed. Sections were fixed in cold 10% formalin pH 7.4 for 15 min and then dehydrated sequentially in 50% ethanol for 5 min, 70% ethanol for 5 min, and 100% ethanol for 10 min at RT. The slides were allowed to dry briefly and hydrophobic boundaries around the tissue sections were drawn with ImmEdge® PAP pen (Vector Laboratories cat. no. H-4000). RNAScope® Fluorescent Multiplex Reagent Kit (Advanced Cell Diagnostics (ACD), cat. no. 323100) was used to detect target *EGR1* and *SCN10A* mRNAs in hDRGs. The sections were treated with hydrogen peroxide (ACD, cat. no. 322335) for 10 min at RT followed by a rinse with ddH_2O. Sections then underwent 5 s of protease III (ACD, cat. no. 322337) digestion followed by a quick wash in 1X PBS pH 7.4 at RT. *EGR1* (Channel 1) and *SCN10A* (Channel 2) probes were mixed in 50:1 ratio. The probe solution was added to the sections which were then placed onto the HybEZ™ Slide Rack (ACD, cat. no. 310017) which was then placed inside the HybEZ™ tray (ACD, cat. no. 310012). Probes were hybridized at 40°C for 2 h in HybEZ™ II Oven (ACD, cat. no. 321721). Sections were rinsed twice in 1X RNAScope® Wash Buffer (ACD, cat. no. 310091) at RT for a couple of minutes each. The sections were stored in 5X SSC buffer (Sigma-Aldrich, cat. no. S6636) overnight at RT. The slides were rinsed twice with 1X wash buffer followed by amplification with Amp 1 for 30 min, Amp 2 for 30 min, and Amp 3 for 15 min at 40°C. Channel 1 probe was coupled with Cy3 for *EGR1* detection and channel 2 with Cy5 for *SCN10A* detection. After rinsing two times with 1X wash buffer, sections were incubated with 1:5000 DAPI in 0.1M PB pH 7.4 for 1 min. Tissue sections underwent a rinse with 0.1M PB pH 7.4 before being air-dried completely and cover-slipped with ProLong™ Gold Antifade Mountant (Fisher Scientific cat. no. P36930).

Slides were imaged at 20X and 100X magnification using the Olympus FV3000 RS confocal laser scanning microscope. *In situ* hybridization analysis was performed using ImageJ Fiji version 2.14.0 by Difference of Gaussians (DoG) edge detection method. ROIs were hand-drawn around each neuron avoiding lipofuscin on the image hyper stack. Channels with target probe were separated from the hyper stack and duplicated. The two images underwent the application of Gaussian Blur with sigma values 1 and 2 respectively. The two resulting images with blurs were subtracted using the built-in Image Calculator feature in ImageJ Fiji which allowed for detection of *in situ* hybridization puncta using the default threshold function. Thresholding values that allowed for as little noise as possible without compromising the signal were chosen for each channel. Analyze Particles feature was used to analyze the number of puncta. The count readout was extracted from the images across the 10 donors which were then used to plot *EGR1* puncta count in *SCN10A* positive or negative neurons for each sex.

Acknowledgements

We acknowledge Yeunhee Kim, Manager of UTD Genome Center for technical support with library prep for RNA-seq and DNA and RNA sequencing. We acknowledge Jennifer Garbarino, Andrés Hernández-Oliveras, Abhira Ravirala and Zawge Yohannes Daniel for the technical support to this project. The authors thank Anna Cervantes, Geoffrey Funk, and Peter Horton at the Southwest Transplant Alliance. The authors are grateful to the organ donors and their families for their gift. This work was supported by NIH grant U19NS130608 and R01NS111929 to TJP.

References

1. Patil M, *et al.* (2019) Prolactin Regulates Pain Responses via a Female-Selective Nociceptor-Specific Mechanism. *iScience* 20:449-465.
2. Berkley KJ (1997) Sex differences in pain. *Behav Brain Sci* 20(3):371-380; discussion 435-513.
3. Greenspan JD, *et al.* (2007) Studying sex and gender differences in pain and analgesia: a consensus report. *Pain* 132 Suppl 1(Suppl 1):S26-S45.
4. Mogil JS (2016) Perspective: Equality need not be painful. *Nature* 535(7611):S7.
5. Mogil JS (2020) Qualitative sex differences in pain processing: emerging evidence of a biased literature. *Nat Rev Neurosci* 21(7):353-365.
6. Mogil JS & Bailey AL (2010) Sex and gender differences in pain and analgesia. *Prog Brain Res* 186:141-157.
7. Rosen S, Ham B, & Mogil JS (2017) Sex differences in neuroimmunity and pain. *J Neurosci Res* 95(1-2):500-508.
8. Tsang A, *et al.* (2008) Common chronic pain conditions in developed and developing countries: gender and age differences and comorbidity with depression-anxiety disorders. *J Pain* 9(10):883-891.
9. Fillingim RB, King CD, Ribeiro-Dasilva MC, Rahim-Williams B, & Riley JL, 3rd (2009) Sex, gender, and pain: a review of recent clinical and experimental findings. *J Pain* 10(5):447-485.
10. Pieretti S, *et al.* (2016) Gender differences in pain and its relief. *Ann Ist Super Sanita* 52(2):184-189.
11. Ghazisaeidi S, Muley MM, & Salter MW (2023) Neuropathic Pain: Mechanisms, Sex Differences, and Potential Therapies for a Global Problem. *Annu Rev Pharmacol Toxicol* 63:565-583.
12. Gregus AM, Levine IS, Eddinger KA, Yaksh TL, & Buczynski MW (2021) Sex differences in neuroimmune and glial mechanisms of pain. *Pain* 162(8):2186-2200.
13. North RY, *et al.* (2019) Electrophysiological and transcriptomic correlates of neuropathic pain in human dorsal root ganglion neurons. *Brain* 142(5):1215-1226.
14. Ray PR, *et al.* (2023) RNA profiling of human dorsal root ganglia reveals sex differences in mechanisms promoting neuropathic pain. *Brain* 146(2):749-766.
15. Ray PR, *et al.* (2019) Transcriptome Analysis of the Human Tibial Nerve Identifies Sexually Dimorphic Expression of Genes Involved in Pain, Inflammation, and Neuro-Immunity. *Front Mol Neurosci* 12:37.
16. Tavares-Ferreira D, *et al.* (2022) Sex Differences in Nociceptor Translatomes Contribute to Divergent Prostaglandin Signaling in Male and Female Mice. *Biol Psychiatry* 91(1):129-140.
17. Tavares-Ferreira D, *et al.* (2022) Spatial transcriptomics of dorsal root ganglia identifies molecular signatures of human nociceptors. *Sci Transl Med* 14(632):eabj8186.
18. Mecklenburg J, *et al.* (2020) Transcriptomic sex differences in sensory neuronal populations of mice. *Sci Rep* 10(1):15278.
19. Lopes DM, *et al.* (2017) Sex differences in peripheral not central immune responses to pain-inducing injury. *Sci Rep* 7(1):16460.
20. Barter MJ, *et al.* (2021) Dynamic chromatin accessibility landscape changes following interleukin-1 stimulation. *Epigenetics* 16(1):106-119.
21. Klemm SL, Shipony Z, & Greenleaf WJ (2019) Chromatin accessibility and the regulatory epigenome. *Nat Rev Genet* 20(4):207-220.
22. Margueron R & Reinberg D (2010) Chromatin structure and the inheritance of epigenetic information. *Nat Rev Genet* 11(4):285-296.
23. Mine-Hattab J & Chiolo I (2020) Complex Chromatin Motions for DNA Repair. *Front Genet* 11:800.

24. Uchida H, Ma L, & Ueda H (2010) Epigenetic gene silencing underlies C-fiber dysfunctions in neuropathic pain. *J Neurosci* 30(13):4806-4814.
25. Chu C*, et al.* (2011) Transcription factors Sp1 and Sp4 regulate TRPV1 gene expression in rat sensory neurons. *Mol Pain* 7:44.
26. Matsushita Y, Araki K, Omotuyi O, Mukae T, & Ueda H (2013) HDAC inhibitors restore C-fibre sensitivity in experimental neuropathic pain model. *Br J Pharmacol* 170(5):991-998.
27. Uchida H, Matsushita Y, & Ueda H (2013) Epigenetic regulation of BDNF expression in the primary sensory neurons after peripheral nerve injury: implications in the development of neuropathic pain. *Neuroscience* 240:147-154.
28. Manners MT, Ertel A, Tian Y, & Ajit SK (2016) Genome-wide redistribution of MeCP2 in dorsal root ganglia after peripheral nerve injury. *Epigenetics Chromatin* 9:23.
29. Stephens KE*, et al.* (2021) Global gene expression and chromatin accessibility of the peripheral nervous system in animal models of persistent pain. *J Neuroinflammation* 18(1):185.
30. Ghosh K & Pan HL (2022) Epigenetic Mechanisms of Neural Plasticity in Chronic Neuropathic Pain. *ACS Chem Neurosci* 13(4):432-441.
31. Laumet G*, et al.* (2015) G9a is essential for epigenetic silencing of K(+) channel genes in acute-to-chronic pain transition. *Nat Neurosci* 18(12):1746-1755.
32. Parisien M*, et al.* (2017) Effect of Human Genetic Variability on Gene Expression in Dorsal Root Ganglia and Association with Pain Phenotypes. *Cell Rep* 19(9):1940-1952.
33. Yang L*, et al.* (2022) Human and mouse trigeminal ganglia cell atlas implicates multiple cell types in migraine. *Neuron* 110(11):1806-1821 e1808.
34. Buenrostro JD, Wu B, Chang HY, & Greenleaf WJ (2015) ATAC-seq: A Method for Assaying Chromatin Accessibility Genome-Wide. *Curr Protoc Mol Biol* 109:21 29 21-21 29 29.
35. Schang AL, Saberan-Djoneidi D, & Mezger V (2018) The impact of epigenomic next-generation sequencing approaches on our understanding of neuropsychiatric disorders. *Clin Genet* 93(3):467-480.
36. Corces MR*, et al.* (2017) An improved ATAC-seq protocol reduces background and enables interrogation of frozen tissues. *Nat Methods* 14(10):959-962.
37. Hauberg ME*, et al.* (2020) Common schizophrenia risk variants are enriched in open chromatin regions of human glutamatergic neurons. *Nat Commun* 11(1):5581.
38. Starks RR, Biswas A, Jain A, & Tuteja G (2019) Combined analysis of dissimilar promoter accessibility and gene expression profiles identifies tissue-specific genes and actively repressed networks. *Epigenetics Chromatin* 12(1):16.
39. Granja JM*, et al.* (2021) ArchR is a scalable software package for integrative single-cell chromatin accessibility analysis. *Nat Genet* 53(3):403-411.
40. Thibodeau A, Uyar A, Khetan S, Stitzel ML, & Ucar D (2018) A neural network based model effectively predicts enhancers from clinical ATAC-seq samples. *Sci Rep* 8(1):16048.
41. Yan F, Powell DR, Curtis DJ, & Wong NC (2020) From reads to insight: a hitchhiker's guide to ATAC-seq data analysis. *Genome Biol* 21(1):22.
42. San Roman AK*, et al.* (2023) The human Y and inactive X chromosomes similarly modulate autosomal gene expression. *bioRxiv*.
43. Sun W, Ma M, Yu H, & Yu H (2018) Inhibition of lncRNA X inactivate-specific transcript ameliorates inflammatory pain by suppressing satellite glial cell activation and inflammation by acting as a sponge of miR-146a to inhibit Na(v) 1.7. *J Cell Biochem* 119(12):9888-9898.
44. Wei M*, et al.* (2019) LncRNA X inactive specific transcript contributes to neuropathic pain development by sponging miR-154-5p via inducing toll-like receptor 5 in CCI rat models. *J Cell Biochem* 120(2):1271-1281.

45. Shenoda BB, *et al.* (2021) Xist attenuates acute inflammatory response by female cells. *Cell Mol Life Sci* 78(1):299-316.
46. Liao J, Zhang F, Qing W, Yu R, & Hu Z (2021) Mechanism of Incisional Pain: Novel Finding on Long Noncoding RNA XIST/miR-340-5p/RAB1A Axis. *ASN Neuro* 13:17590914211049056.
47. Heydari R, *et al.* (2022) Y chromosome is moving out of sex determination shadow. *Cell Biosci* 12(1):4.
48. Bentsen M, *et al.* (2020) ATAC-seq footprinting unravels kinetics of transcription factor binding during zygotic genome activation. *Nat Commun* 11(1):4267.
49. Huang ZZ, *et al.* (2014) CX3CL1-mediated macrophage activation contributed to paclitaxel-induced DRG neuronal apoptosis and painful peripheral neuropathy. *Brain Behav Immun* 40:155-165.
50. Obeidat AM, *et al.* (2023) Piezo2 expressing nociceptors mediate mechanical sensitization in experimental osteoarthritis. *Nat Commun* 14(1):2479.
51. Qiu F, *et al.* (2014) Oxytocin inhibits the activity of acid-sensing ion channels through the vasopressin, V1A receptor in primary sensory neurons. *Br J Pharmacol* 171(12):3065-3076.
52. Gong L, *et al.* (2015) Oxytocin-induced membrane hyperpolarization in pain-sensitive dorsal root ganglia neurons mediated by Ca(2+)/nNOS/NO/KATP pathway. *Neuroscience* 289:417-428.
53. Deng Y, *et al.* (2022) Spatial profiling of chromatin accessibility in mouse and human tissues. *Nature* 609(7926):375-383.
54. Buenrostro JD, Giresi PG, Zaba LC, Chang HY, & Greenleaf WJ (2013) Transposition of native chromatin for fast and sensitive epigenomic profiling of open chromatin, DNA-binding proteins and nucleosome position. *Nat Methods* 10(12):1213-1218.
55. Nguyen MQ, von Buchholtz LJ, Reker AN, Ryba NJ, & Davidson S (2021) Single-nucleus transcriptomic analysis of human dorsal root ganglion neurons. *Elife* 10.
56. Bhuiyan SA, *et al.* (2023) Harmonized cross-species cell atlases of trigeminal and dorsal root ganglia. *bioRxiv*.
57. Jung M, *et al.* (2023) Cross-species transcriptomic atlas of dorsal root ganglia reveals species-specific programs for sensory function. *Nat Commun* 14(1):366.
58. Kuleshov MV, *et al.* (2016) Enrichr: a comprehensive gene set enrichment analysis web server 2016 update. *Nucleic Acids Res* 44(W1):W90-97.
59. Herman AB, Tsitsipatis D, & Gorospe M (2022) Integrated lncRNA function upon genomic and epigenomic regulation. *Mol Cell* 82(12):2252-2266.
60. Sas-Nowosielska H & Magalska A (2021) Long Noncoding RNAs-Crucial Players Organizing the Landscape of the Neuronal Nucleus. *Int J Mol Sci* 22(7).
61. Zaghlool A, *et al.* (2021) Characterization of the nuclear and cytosolic transcriptomes in human brain tissue reveals new insights into the subcellular distribution of RNA transcripts. *Sci Rep* 11(1):4076.
62. Ito S, Das ND, Umehara T, & Koseki H (2022) Factors and Mechanisms That Influence Chromatin-Mediated Enhancer-Promoter Interactions and Transcriptional Regulation. *Cancers (Basel)* 14(21).
63. Popova BC, Tada T, Takagi N, Brockdorff N, & Nesterova TB (2006) Attenuated spread of X-inactivation in an X;autosome translocation. *Proc Natl Acad Sci U S A* 103(20):7706-7711.
64. Rodermund L, *et al.* (2021) Time-resolved structured illumination microscopy reveals key principles of Xist RNA spreading. *Science* 372(6547).
65. Schwammle T & Schulz EG (2023) Regulatory principles and mechanisms governing the onset of random X-chromosome inactivation. *Curr Opin Genet Dev* 81:102063.
66. Patrat C, Ouimette JF, & Rougeulle C (2020) X chromosome inactivation in human development. *Development* 147(1).

67. Balaton BP & Brown CJ (2016) Escape Artists of the X Chromosome. *Trends Genet* 32(6):348-359.
68. Tukiainen T, *et al.* (2017) Landscape of X chromosome inactivation across human tissues. *Nature* 550(7675):244-248.
69. Wen X, *et al.* (2024) Single-cell multiplex chromatin and RNA interactions in ageing human brain. *Nature*.
70. Shiers S, *et al.* (2020) ACE2 and SCARF expression in human dorsal root ganglion nociceptors: implications for SARS-CoV-2 virus neurological effects. *Pain* 161(11):2494-2501.
71. Yu S, *et al.* (2019) Genes known to escape X chromosome inactivation predict co-morbid chronic musculoskeletal pain and posttraumatic stress symptom development in women following trauma exposure. *Am J Med Genet B Neuropsychiatr Genet* 180(6):415-427.
72. Franco-Enzastiga U, *et al.* (2022) Extrasynaptic α5GABAA receptors and their role in nociception and pathological pain. *The Neurobiology, Physiology, and Psychology of Pain*, eds Rajendram R, Preedy VR, Patel V, & Martin CR (Academic Press), pp 129-137.
73. Franco-Enzastiga U, *et al.* (2021) Sex-dependent pronociceptive role of spinal alpha(5) -GABA(A) receptor and its epigenetic regulation in neuropathic rodents. *J Neurochem* 156(6):897-916.
74. Latremoliere A & Woolf CJ (2009) Central sensitization: a generator of pain hypersensitivity by central neural plasticity. *J Pain* 10(9):895-926.
75. Coull JA, *et al.* (2005) BDNF from microglia causes the shift in neuronal anion gradient underlying neuropathic pain. *Nature* 438(7070):1017-1021.
76. Mapplebeck JCS, *et al.* (2019) Chloride Dysregulation through Downregulation of KCC2 Mediates Neuropathic Pain in Both Sexes. *Cell Rep* 28(3):590-596 e594.
77. Moy JK, *et al.* (2019) Temporal and sex differences in the role of BDNF/TrkB signaling in hyperalgesic priming in mice and rats. *Neurobiol Pain* 5:100024.
78. Dedek A, *et al.* (2022) Sexual dimorphism in a neuronal mechanism of spinal hyperexcitability across rodent and human models of pathological pain. *Brain* 145(3):1124-1138.
79. Woodson CM & Kehn-Hall K (2022) Examining the role of EGR1 during viral infections. *Front Microbiol* 13:1020220.
80. Duclot F & Kabbaj M (2017) The Role of Early Growth Response 1 (EGR1) in Brain Plasticity and Neuropsychiatric Disorders. *Front Behav Neurosci* 11:35.
81. Rocks D, *et al.* (2023) Egr1 is a sex-specific regulator of neuronal chromatin, synaptic plasticity, and behaviour. *bioRxiv*.
82. Barragan-Iglesias P, *et al.* (2019) Activation of the integrated stress response in nociceptors drives methylglyoxal-induced pain. *Pain* 160(1):160-171.
83. Franco-Enzastiga U, *et al.* (2024) Vinorelbine causes a neuropathic pain-like state in mice via STING and MNK1 signaling associated with type I interferon induction. *iScience* 27(2):108808.
84. Sheehan K, *et al.* (2019) Transcription factor Sp4 is required for hyperalgesic state persistence. *PLoS One* 14(2):e0211349.
85. Xu Z, *et al.* (2024) Chemotherapy for pain: reversing inflammatory and neuropathic pain with the anticancer agent mithramycin A. *Pain* 165(1):54-74.
86. Stephens KE, *et al.* (2019) Sex differences in gene regulation in the dorsal root ganglion after nerve injury. *BMC Genomics* 20(1):147.
87. Janssens DH, *et al.* (2024) Scalable single-cell profiling of chromatin modifications with sciCUT&Tag. *Nat Protoc* 19(1):83-112.
88. Marquez EJ, *et al.* (2020) Sexual-dimorphism in human immune system aging. *Nat Commun* 11(1):751.
89. Valtcheva MV, *et al.* (2016) Surgical extraction of human dorsal root ganglia from organ donors and preparation of primary sensory neuron cultures. *Nat Protoc* 11(10):1877-1888.

90. Mich JK, *et al.* (2021) Functional enhancer elements drive subclass-selective expression from mouse to primate neocortex. *Cell Rep* 34(13):108754.
91. Zhang H, *et al.* (2021) Fast alignment and preprocessing of chromatin profiles with Chromap. *Nat Commun* 12(1):6566.

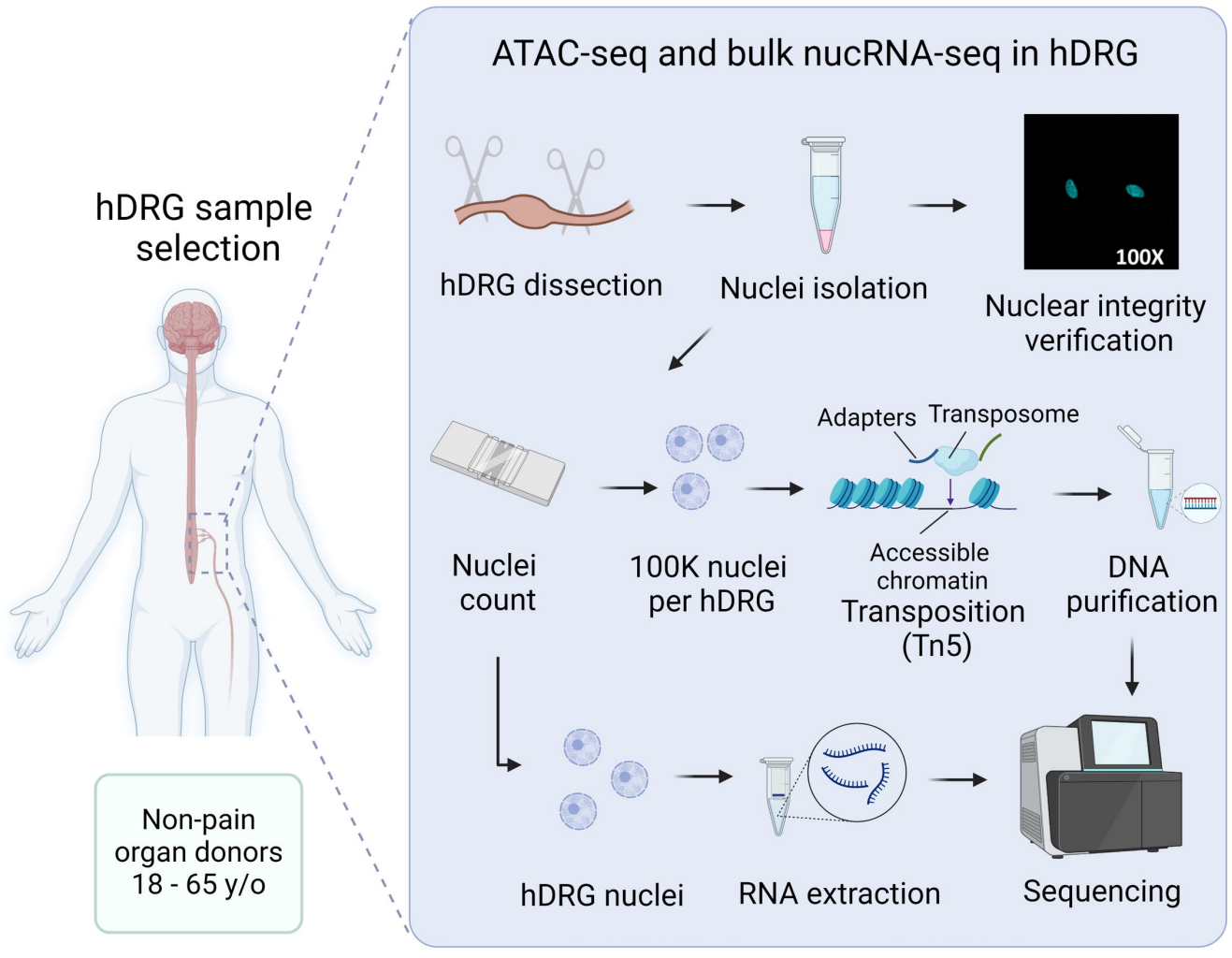
A
hDRG sample selection
Non-pain organ donors 18 - 65 y/o
ATAC-seq and bulk nucRNA-seq in hDRG
hDRG dissection
Nuclei isolation
100X
Nuclear integrity verification
Nuclei count
100K nuclei per hDRG
Adapters
Transposome
Accessible chromatin
Transposition (Tn5)
DNA purification
hDRG nuclei
RNA extraction
Sequencing

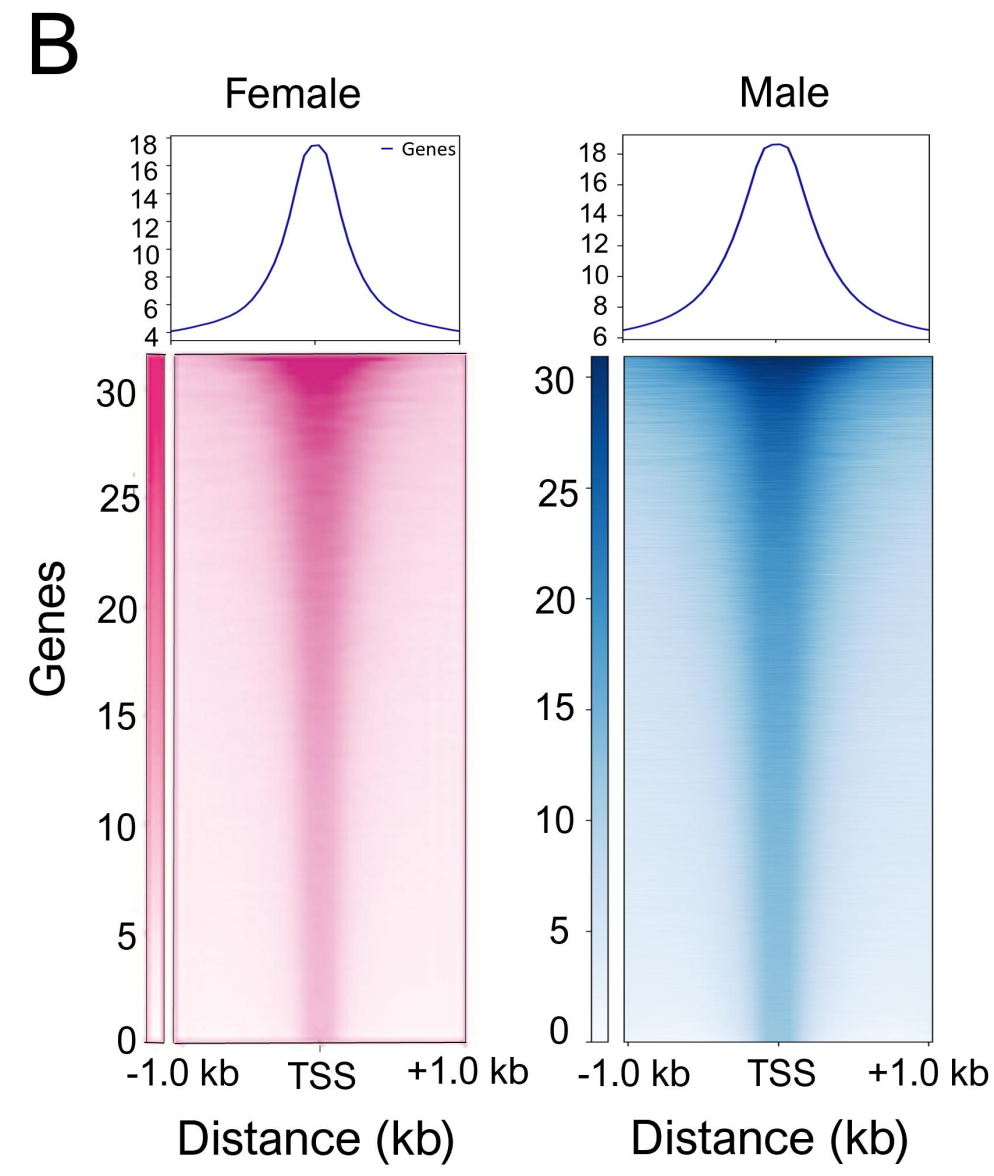
B
Female
Male
Genes
Genes
-1.0 kb
TSS
+1.0 kb
Distance (kb)

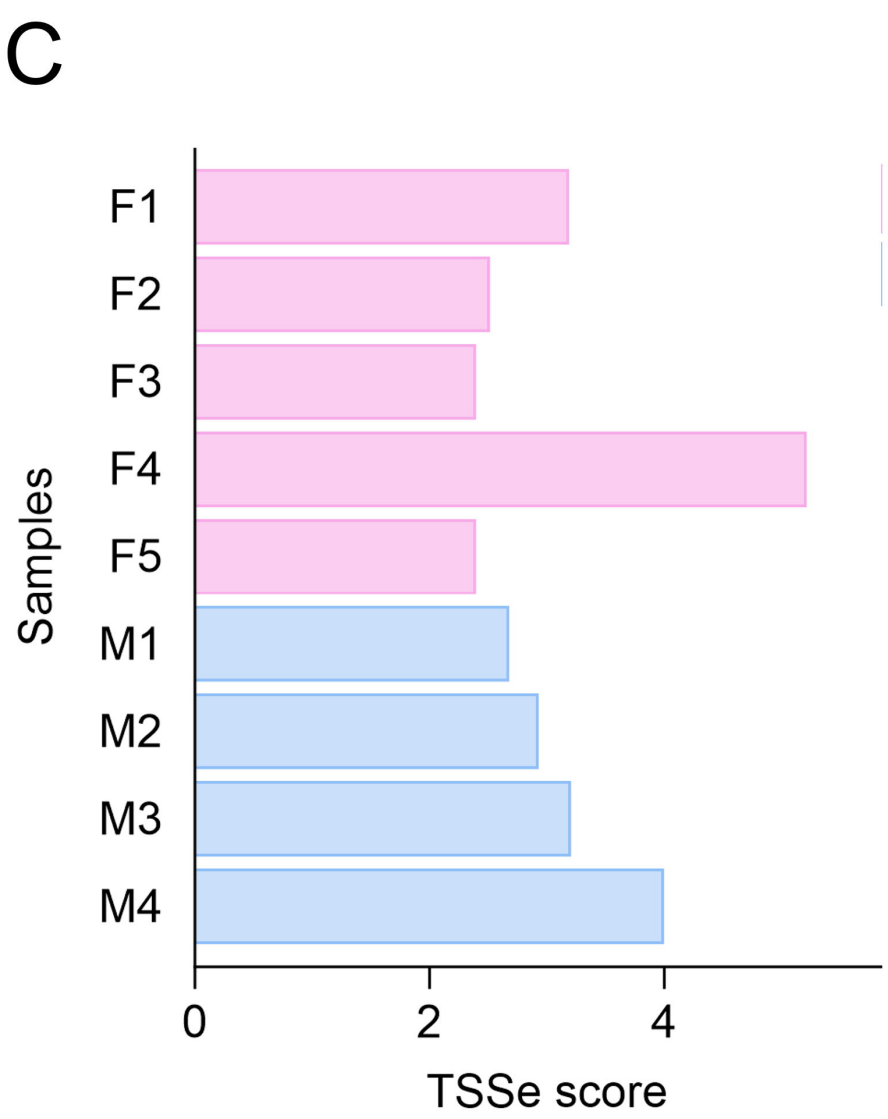
C
Samples
F1
F2
F3
F4
F5
M1
M2
M3
M4
0
2
4
TSSe score

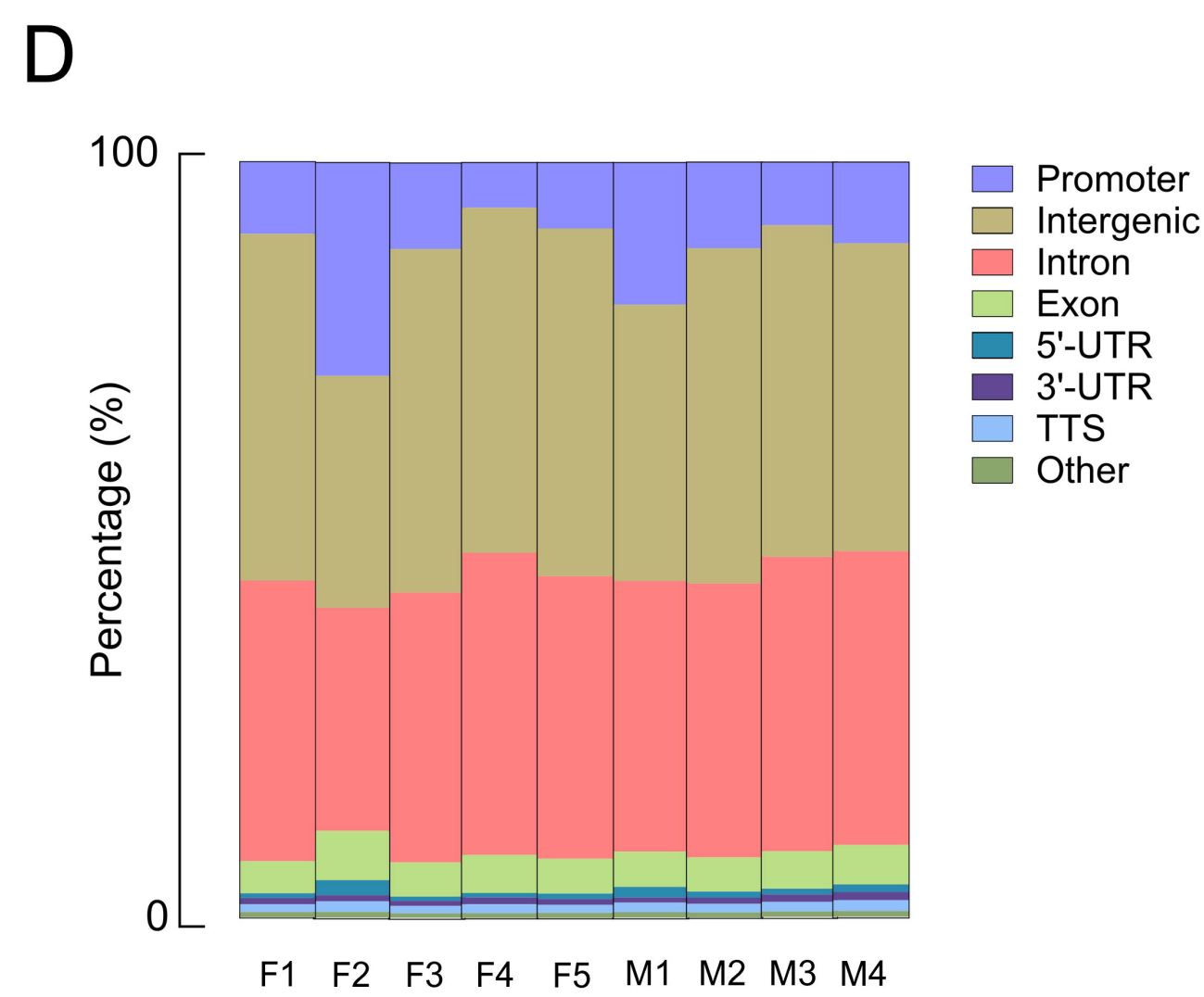
D
100
0
Percentage (%)
F1
F2
F3
F4
F5
M1
M2
M3
M4
Promoter
Intergenic
Intron
Exon
5'-UTR
3'-UTR
TTS
Other

A

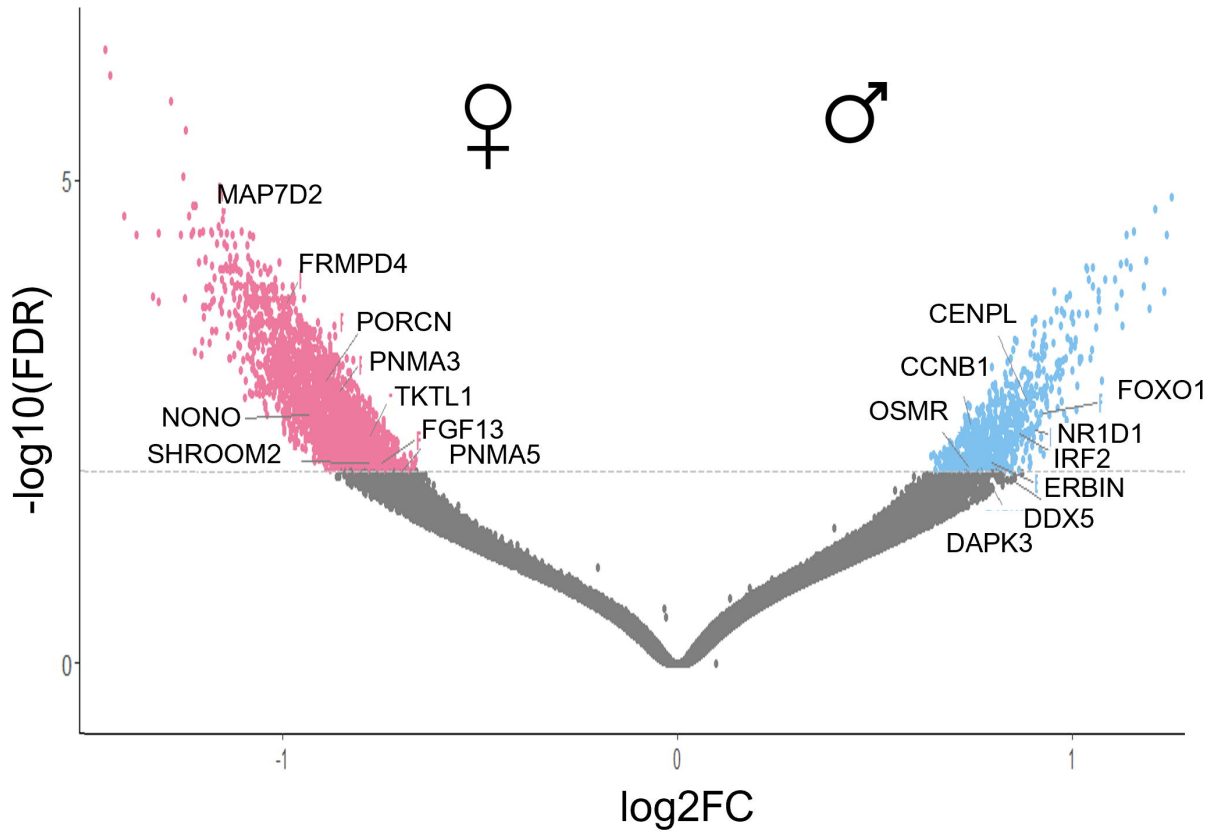

B

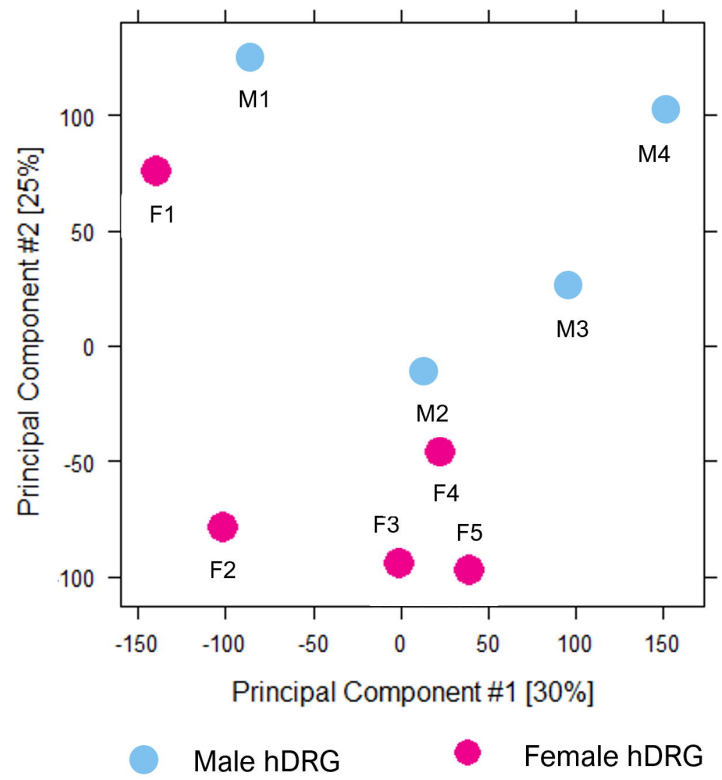

C

Female enriched peaks

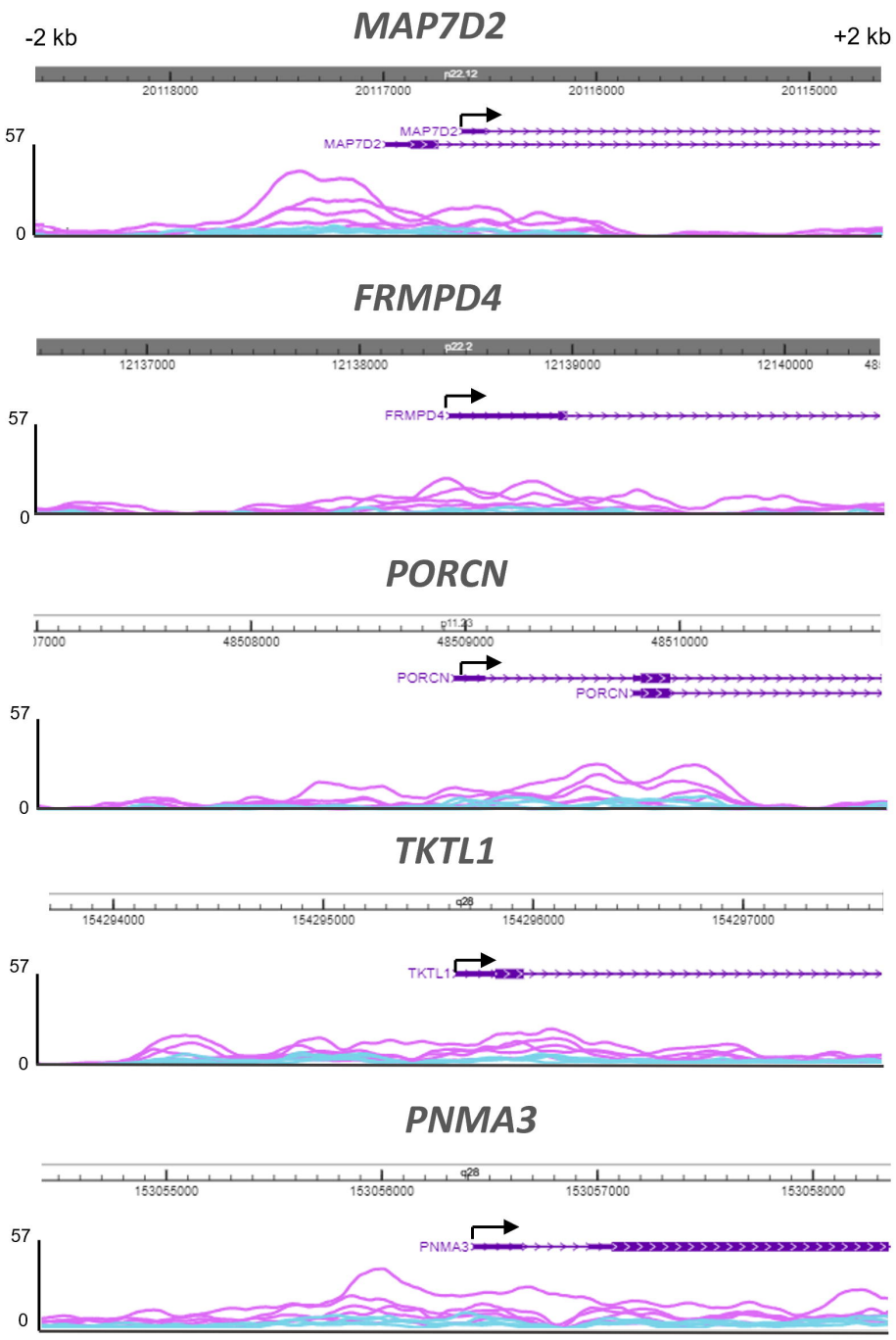

D

Male enriched peaks

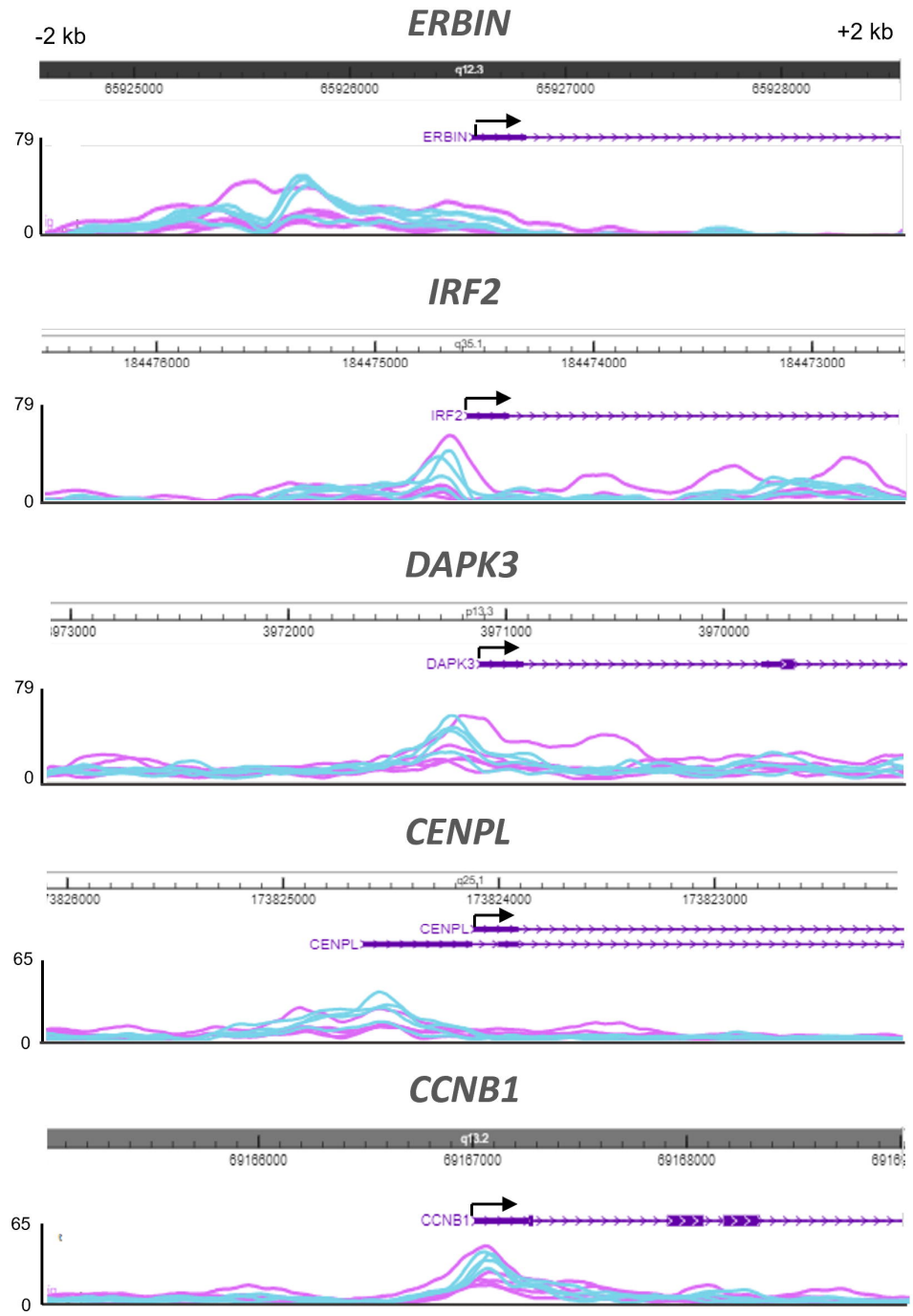

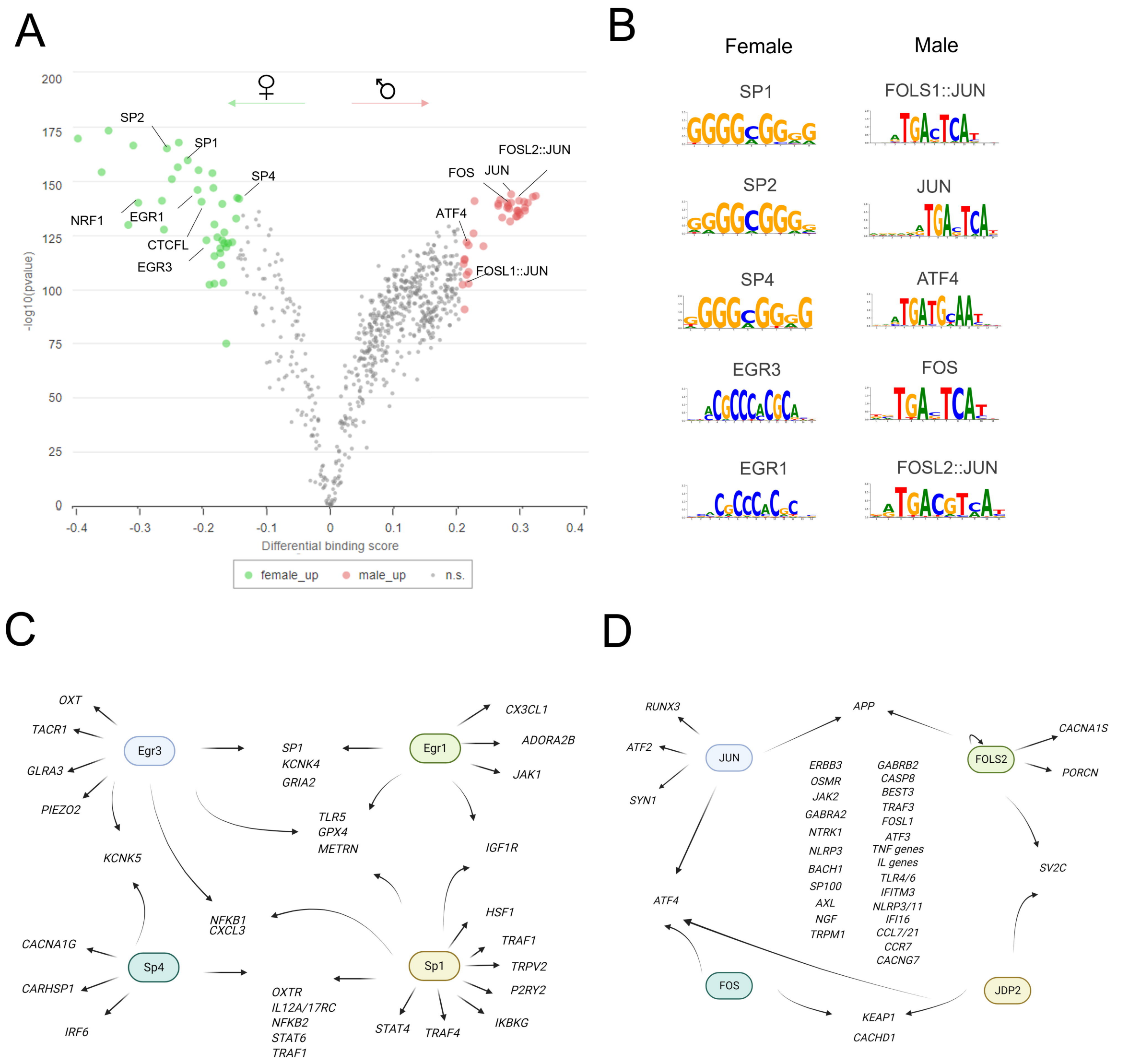
A
♀
♂
SP2
SP1
SP4
NRF1
EGR1
CTCFL
EGR3
FOS
JUN
FOSL2::JUN
ATF4
FOSL1::JUN
-log10(pvalue)
Differential binding score
female_up
male_up
n.s.
B
Female
Male
SP1
FOLS1::JUN
SP2
JUN
SP4
ATF4
EGR3
FOS
EGR1
FOSL2::JUN
C
Egr3
OXT
TACR1
GLRA3
PIEZO2
KCNK5
SP1
KCNK4
GRIA2
TLR5
GPX4
METRN
Egr1
CX3CL1
ADORA2B
JAK1
IGF1R
NFKB1
CXCL3
Sp4
CACNA1G
CARHSP1
IRF6
OXTR
IL12A/17RC
NFKB2
STAT6
TRAF1
Sp1
HSF1
TRAF1
TRPV2
P2RY2
IKBKG
STAT4
TRAF4
D
RUNX3
ATF2
SYN1
JUN
APP
ATF4
ERBB3
OSMR
JAK2
GABRA2
NTRK1
NLRP3
BACH1
SP100
AXL
NGF
TRPM1
GABRB2
CASP8
BEST3
TRAF3
FOSL1
ATF3
TNF genes
IL genes
TLR4/6
IFITM3
NLRP3/11
IFI16
CCL7/21
CCR7
CACNG7
FOLS2
CACNA1S
PORCN
SV2C
FOS
JDP2
KEAP1
CACHD1

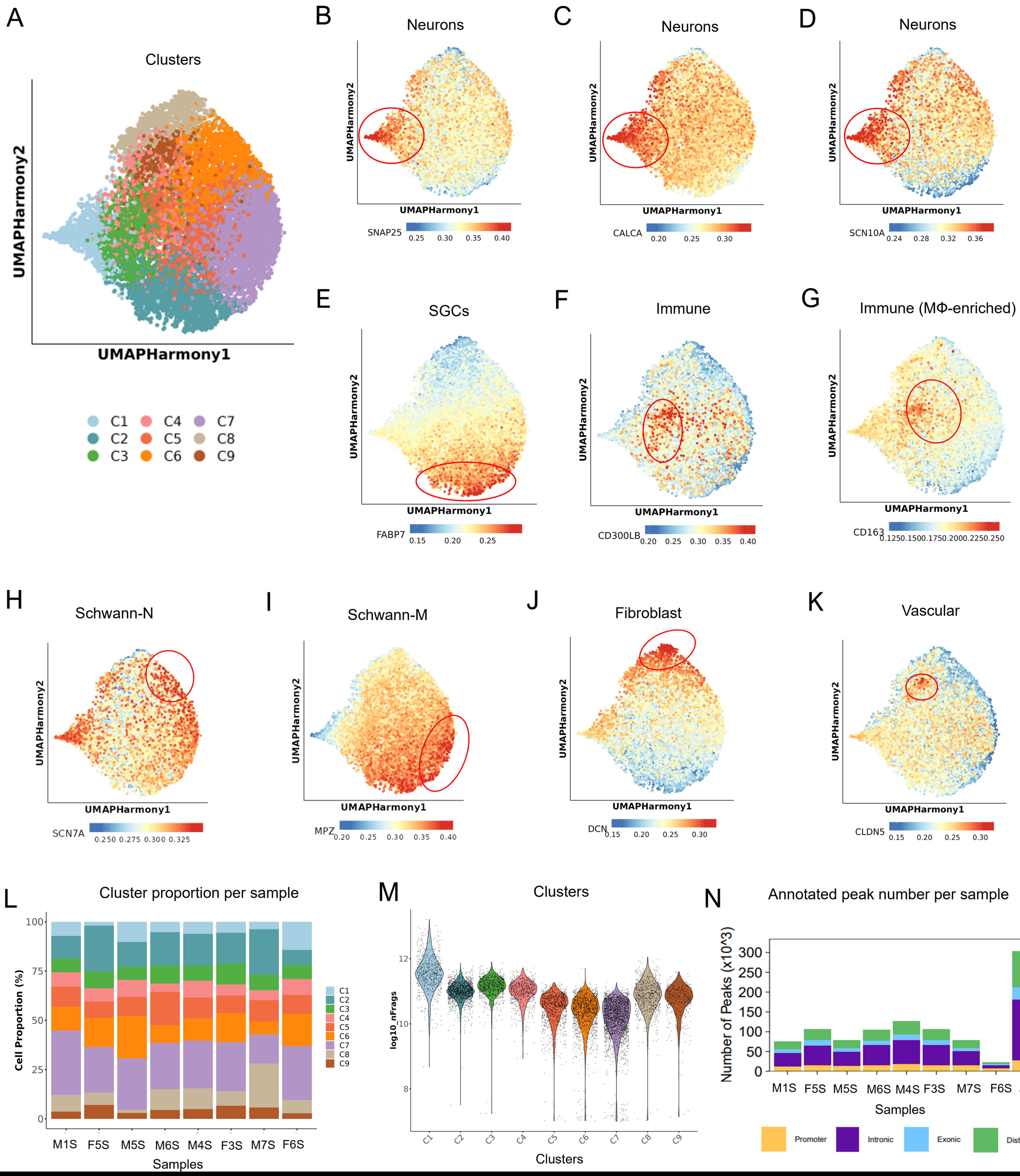
A
Clusters
UMAPHarmony2
UMAPHarmony1
C1 C4 C7
C2 C5 C8
C3 C6 C9
B
Neurons
SNAP25
0.25 0.30 0.35 0.40
C
Neurons
CALCA
0.20 0.25 0.30
D
Neurons
SCN10A
0.24 0.28 0.32 0.36
E
SGCs
FABP7
0.15 0.20 0.25
F
Immune
CD300LB
0.20 0.25 0.30 0.35 0.40
G
Immune (MΦ-enriched)
CD163
0.1250.1500.1750.2000.2250.250
H
Schwann-N
SCN7A
0.250 0.275 0.300 0.325
I
Schwann-M
MPZ
0.20 0.25 0.30 0.35 0.40
J
Fibroblast
DCN
0.15 0.20 0.25 0.30
K
Vascular
CLDN5
0.15 0.20 0.25 0.30
L
Cluster proportion per sample
Cell Proportion (%)
M1S F5S M5S M6S M4S F3S M7S F6S
Samples
M
Clusters
log10_nFrags
Clusters
N
Annotated peak number per sample
Number of Peaks (x10^3)
M1S F5S M5S M6S M4S F3S M7S F6S All
Samples
Promoter
Intronic
Exonic
Distal

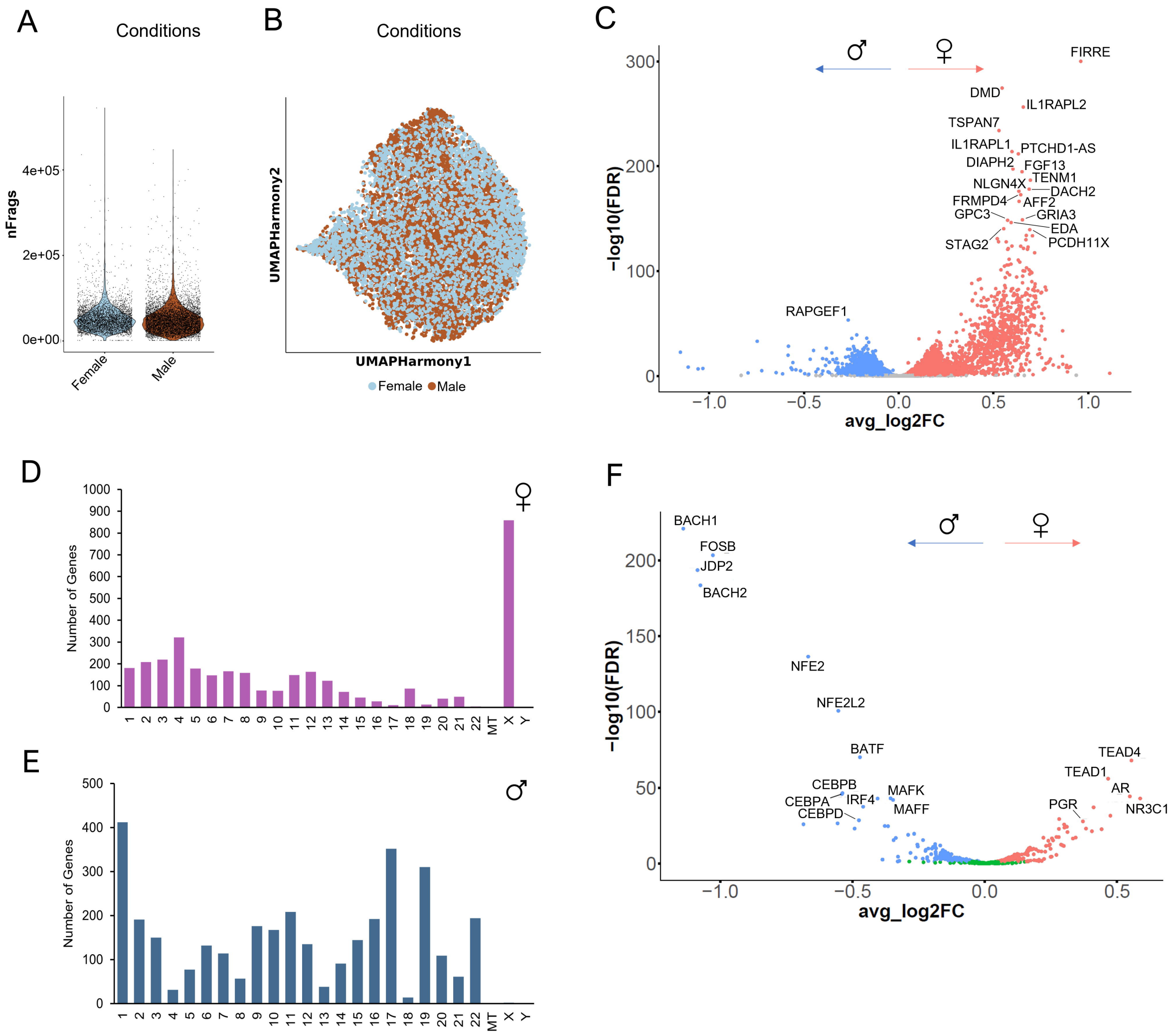
A
Conditions
nFrags
4e+05
2e+05
0e+00
Female
Male
B
Conditions
UMAPHarmony2
UMAPHarmony1
Female
Male
C
♂
♀
FIRRE
DMD
IL1RAPL2
TSPAN7
IL1RAPL1
PTCHD1-AS
DIAPH2
FGF13
TENM1
NLGN4X
DACH2
FRMPD4
AFF2
GPC3
GRIA3
EDA
STAG2
PCDH11X
RAPGEF1
−log10(FDR)
avg_log2FC
D
Number of Genes
E
Number of Genes
F
BACH1
FOSB
JDP2
BACH2
NFE2
NFE2L2
BATF
CEBPB
CEBPA
CEBPD
IRF4
MAFK
MAFF
TEAD4
TEAD1
AR
PGR
NR3C1
−log10(FDR)
avg_log2FC

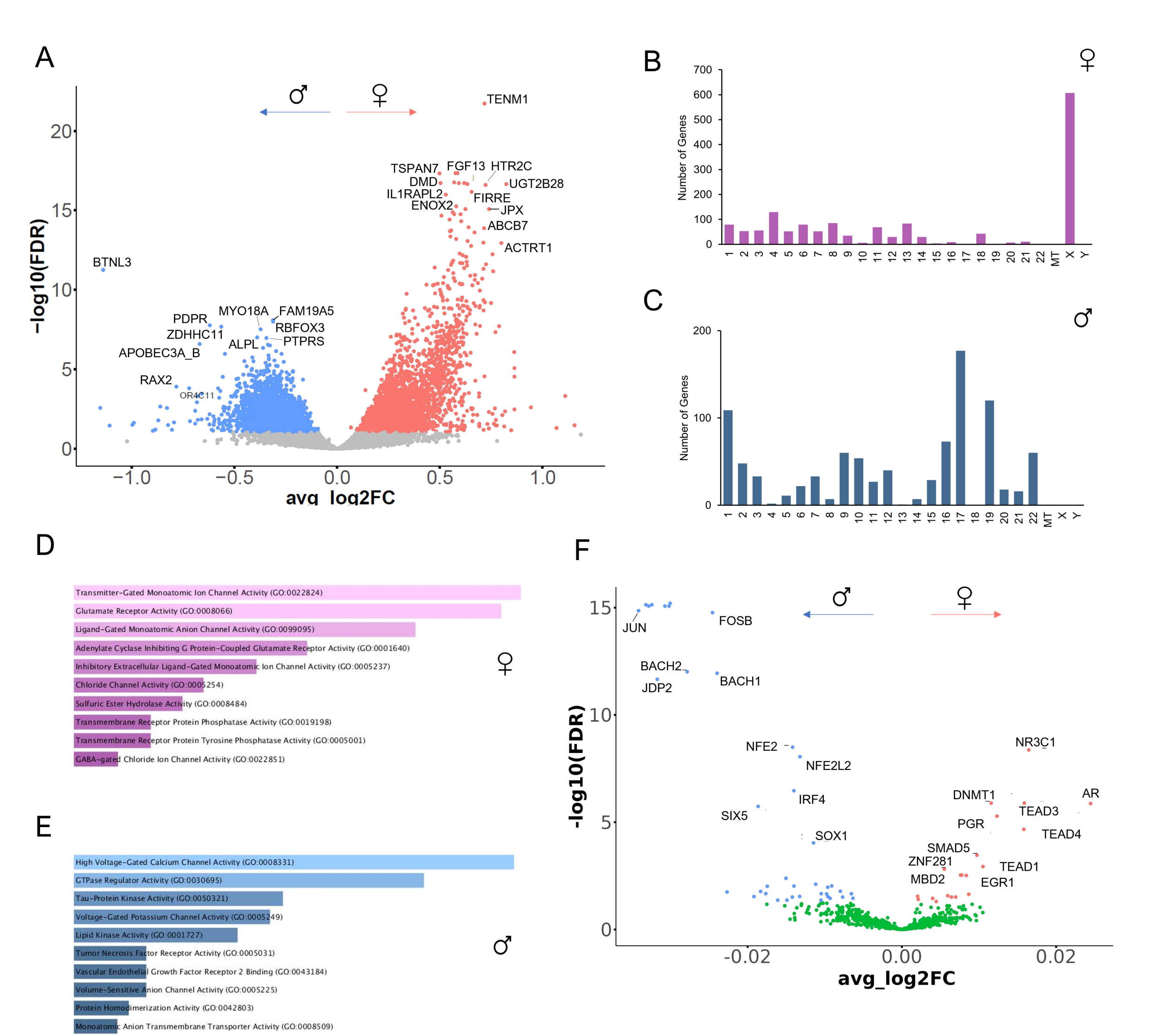
A
♂
♀
TENM1
TSPAN7
FGF13
HTR2C
DMD
UGT2B28
IL1RAPL2
FIRRE
ENOX2
JPX
ABCB7
ACTRT1
BTNL3
MYO18A
FAM19A5
PDPR
RBFOX3
ZDHHC11
ALPL
PTPRS
APOBEC3A_B
RAX2
OR4C11
−log10(FDR)
avg_log2FC
B
♀
Number of Genes
C
♂
Number of Genes
D
Transmitter-Gated Monoatomic Ion Channel Activity (GO:0022824)
Glutamate Receptor Activity (GO:0008066)
Ligand-Gated Monoatomic Anion Channel Activity (GO:0099095)
Adenylate Cyclase Inhibiting G Protein-Coupled Glutamate Receptor Activity (GO:0001640)
Inhibitory Extracellular Ligand-Gated Monoatomic Ion Channel Activity (GO:0005237)
Chloride Channel Activity (GO:0005254)
Sulfuric Ester Hydrolase Activity (GO:0008484)
Transmembrane Receptor Protein Phosphatase Activity (GO:0019198)
Transmembrane Receptor Protein Tyrosine Phosphatase Activity (GO:0005001)
GABA-gated Chloride Ion Channel Activity (GO:0022851)
♀
E
High Voltage-Gated Calcium Channel Activity (GO:0008331)
GTPase Regulator Activity (GO:0030695)
Tau-Protein Kinase Activity (GO:0050321)
Voltage-Gated Potassium Channel Activity (GO:0005249)
Lipid Kinase Activity (GO:0001727)
Tumor Necrosis Factor Receptor Activity (GO:0005031)
Vascular Endothelial Growth Factor Receptor 2 Binding (GO:0043184)
Volume-Sensitive Anion Channel Activity (GO:0005225)
Protein Homodimerization Activity (GO:0042803)
Monoatomic Anion Transmembrane Transporter Activity (GO:0008509)
♂
F
♂
♀
JUN
FOSB
BACH2
JDP2
BACH1
NFE2
NFE2L2
NR3C1
IRF4
DNMT1
AR
SIX5
TEAD3
PGR
TEAD4
SOX1
SMAD5
ZNF281
TEAD1
MBD2
EGR1
-log10(FDR)
avg_log2FC

A

B

EGR1

SCN10A

MERGE + DAPI

EGR1 in SCN10A (+)

FEMALE

MALE

C

D

E
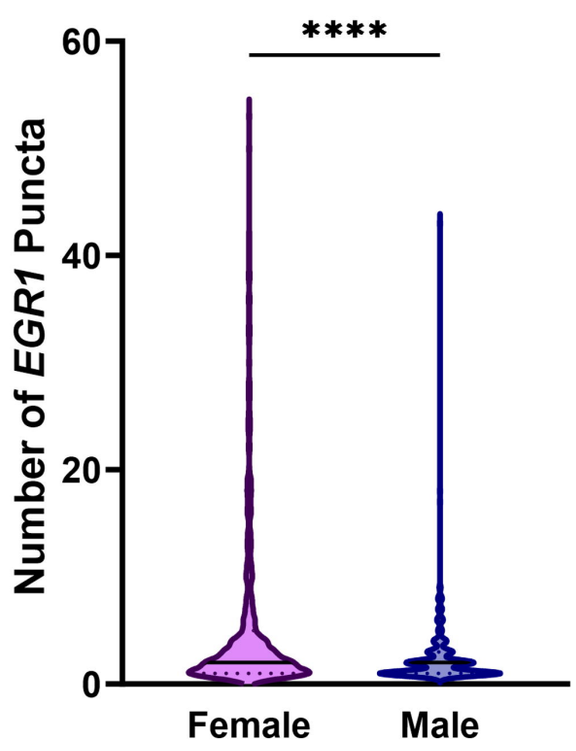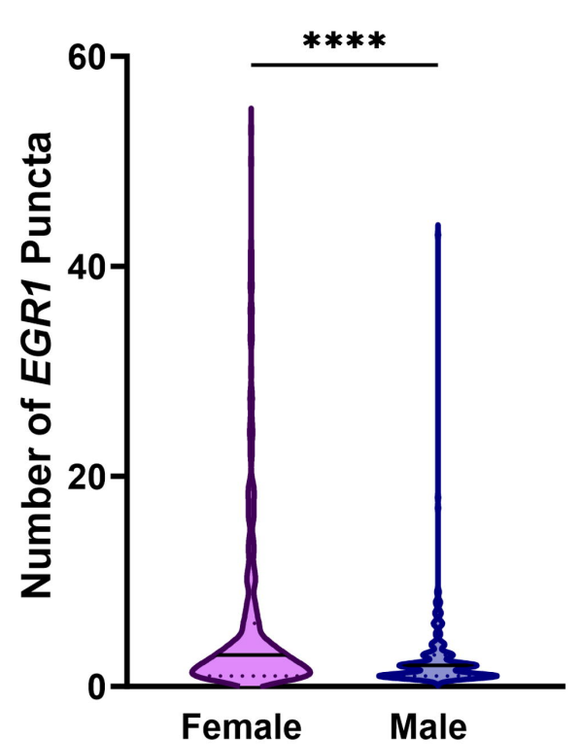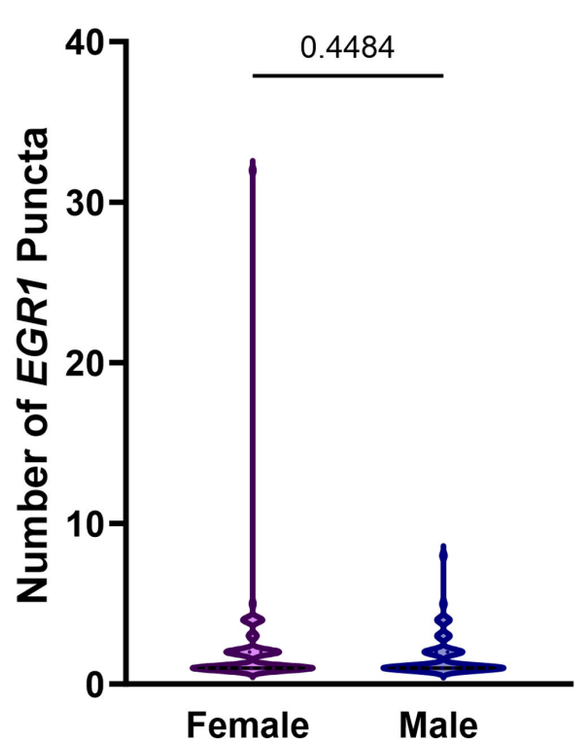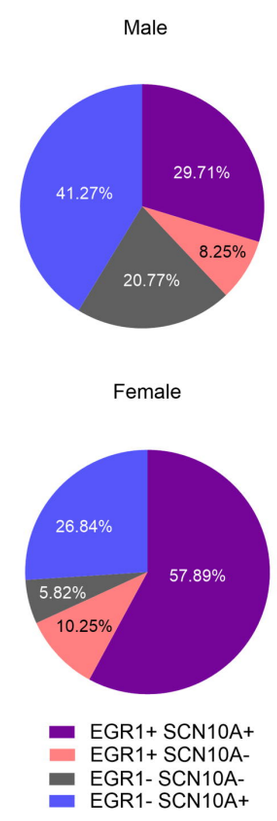
F